Mouse pre-meiotic germline cysts contain fusome-like structure dependent on Dazl that mediates cyst fragmentation and oocyte development

Madhulika Pathak[1] and Allan C. Spradling[1,2]

[1]Howard Hughes Medical Institute Research Laboratories

Carnegie Institution for Science, Baltimore, MD 21218, USA

[2]Lead contact, to whom correspondence should be addressed

ABSTRACT

Mouse female primordial germ cells undergo five synchronous, incomplete mitotic divisions, and send each resulting germline cyst into meiosis to fragment and produce 4-6 oocytes and 24-26 supportive nurse cells. How oocytes are specified, linked appropriately to nurse cells and enabled to acquire high quality organelles and cytoplasm on a massive scale remains unclear. We identified an asymmetric Golgi, ER and microtubule-associated structure, “Visham,” similar to the Drosophila fusome. Starting as the EMA granule, Visham distributes asymmetrically in cyst cells and enriches in future oocytes with Pard3, and Golgi-endosomal UPR (unfolded protein response) genes. Transient spindle remnants rich in stable acetylated microtubules link early cyst cells for part of each cell cycle. Cysts sometimes develop a gap in these microtubules beginning at the 8-cell stage that predicts programmed cyst fragmentation into six-cell cysts of similar structure. Visham persists during meiosis where it mediates Pard3-dependent polarity, Xbp1-dependent adaptive UPR , and organelle transfer to the Balbiani body. In DAZL mutants, cysts still form, but polarity and oocyte production are blocked.

INTRODUCTION

Early female germ cell development occurs within interconnected cysts formed by consecutive incomplete divisions of a germline stem cell (GSC) or PGC in diverse animals. These include basal species like hydra (Littlefield, 1994), nematodes like C. elegans, insects like Drosophila, and vertebrates including fish, frogs, mice and humans (Gondos, 1973; King, 1970; Pepling and Spradling, 1998; Kloc et al. 2004a; Marlow and Mullins, 2008; review, Spradling, 2024). As they develop, cysts acquire polarity and asymmetry that in some species is revealed by a microtubule-rich structure known as the "fusome," meaning spindle-derived (Giardina, 1901,

Huynh and St Johnston, 2004; Spradling et al. 2022). In Drosophila, the fusome is produced from mitotic spindle remnants, contains ER cisternae and is essential for oocyte production. Beginning in pachytene, the fusome changes shape and microtubule polarity. It subsequently mediates the movement of centrioles, mitochondria, and germ plasm regulators such as oskar mRNA toward the oocyte where they enter and form the Balbiani body (Bb) as follicles form. Remarkably, mammalian oocytes also develop from germline cysts, and undergo many steps in common with Drosophila, including the movement of organelles from nurse cells into the oocyte to establish a Balbiani body (review: Spradling et al. 2022).

In the mouse, germ cells are induced around embryonic day 6.5 (E6.5) (Lawson et al. 2002) and begin migrating toward the gonad as primordial germ cells (PGCs). En route, PGCs reprogram their epigenetic state and return to pluripotency (Seki et al. 2007; Saitou et al. 2011; Loda et al. 2022; Liu et al. 2025). However, after they enter the gonad at E10.5, PGCs turn on DDX4 and initiate cyst formation while reprogramming is still ongoing. During E11.5 they upregulate Dazl, an RNA-binding, post-transcriptional regulatory protein which is needed to produce and translate multiple target mRNAs (Huang et al., 2024, Zagore et al., 2018). Dazl plays an essential role promoting germ cell meiotic entry and oocyte production (Gill et al. 2011; Nicholls et al. 2019; Hancock et al. 2021).

Mouse germline cysts arise from five rounds of mitotic divisions that begin at E10.5, so that each PGC generates almost 32 cells. However, the cysts break into an average of 4.8 smaller cysts by the time divisions are completed at E14.5 and cells enter meiosis (Lei and Spradling, 2013; Levy et al. 2024). During meiosis, each smaller cyst slowly loses component cells, as every 2 days about one cell on average becomes activated to act as a nurse cell. It transfers most of its cytoplasm into the residual cyst, shrinks to a small remnant and undergoes programmed

cell death (Lei et al. 2016; Niu and Spradling, 2022; Ikami et al 2023). In pachytene, there is a substantial reorganization that brings mitochondria and ER sheets into close proximity by E18.5 (Pepling and Spradling, 2001). Cyst breakdown is complete by 5 days after birth (P5) with the formation of 4-6 primordial follicles, each containing a single oocyte in which organelles transferred from nurse cells are gathered into a large aggregate known as the Balbiani body. As in Drosophila, cyst polarity is thought to guide oocyte specification, cyst fragmentation, nurse cell activation, and oocyte organelle acquisition, but a mouse analog of the fusome has not been identified.

Germline cysts have also been implicated in germ cell rejuvenation, the universal process that allows damage to be removed each generation so that species can persist without known limit. Germline rejuvenation takes place during meiosis in single celled eukaryotes (Unal et al. 2011; King et al. 2023; Suda et al. 2024). Processes that rejuvenate organelles such as mitochondria, restore rDNA copy number, and reset epigenetic chromatin marks have also been documented in meiosis during animal gametogenesis (Cox and Spradling, 2003; Hill et al. 2014; Reik and Surani, 2015; Bohnert and Kenyon, 2017; Lieber et al. 2019, Pang et al. 2023; Yamashita, 2023). The Balbiani body, in newly formed oocytes, is associated with germ plasm formation and selection for mitochondrial function in many species (Heasman et al. 1984; Kloc et al. 2004b; Marlow and Mullins, 2008; Spradling et al. 2022; Sekula et al. 2024).

Here we find that mouse PGCs and cyst cells elaborate a fusome-like structure we term "Visham" that is rich Golgi, endosomal vesicles and associates with ER. Visham distributes asymmetrically in association with stable microtubules that persist briefly for part of the cyst cell cycle. By the 8 cell stage, cyst cells reorganize into a rosette configuration that brings cells with the most bridges (potential oocytes) and associated Visham closer together. Developing cysts at

this stage frequently fragment non-randomly at sites lacking microtubule connections into six-cell cysts, implying that mouse ovarian cyst structure is more highly controlled than previously realized. Beginning as PGCs and throughout cyst formation, EGAD-mediated UPR pathway proteins including Xbp1 are expressed, suggesting that the oocyte proteome quality begins to be enhanced beginning very early. After pachytene, centrosome/Gogli-rich elements move to the oocyte and mediate the acquisition of organelles by the Bb. In the absence of Dazl, cyst development and asymmetric Visham accumulation is disrupted, and no oocytes are produced.

RESULTS

PGCs contain a Golgi-rich structure known as the EMA granule

Early observations of an "epithelial membrane antigen (EMA)" (Hahnel and Eddy, 1986) identified an "EMA granule" in mouse primordial germ cells that resembles the Drosophila spectrosome, a fusome precursor (Lin et al., 1994; Pepling et al. 1998). To investigate this relationship further, we determined that the EMA-rich structure appears in PGCs as early as E9.5, and continues to be expressed both at the membrane and in one large oval-shaped cluster per cell in PGCs and individual cyst cells as late as E12.5 (Figure 1A, Figure S1A). We used lineage labeling at E10.5 to mark cysts derived from single PGCs, and 3D surface rendering (Fig S1B-C) and volume quantification, which revealed a significantly uneven distribution of the EMA aggregate within the cyst daughter cells (Fig 1B). This structural asymmetry prompted us to name the EMA-rich structure "Visham" (Sanskrit for asymmetric/uneven).

By E13.5 most female cysts, some of which had undergone a breakage event, showed a different pattern in which the clusters of EMA-rich material in each cyst cell were closer to each other (Figure 1C; Figure S1D-E), whereas in male cysts they remained mostly separate (Figure 1C' and graph). We used Tex14 antibody to label the intercellular bridges connecting cell pairs. 8-cell and larger cysts always have one or more branches, connecting a cell to 3 different sister cells. This can be recognized by the presence of 3 spots of Tex14 staining (Figure 1D-D', S1F). Using lineage labeling and Imaris analysis, we found that at E13.5, cyst regions with enriched Visham staining are associated with an average of 3 Tex14-positive bridges, whereas unenriched zones had an average of just 1 (Figure 1D graph). Thus, highly branched cells with more bridges, which are known to give rise to most oocytes (Lei and Spradling, 2013; Lei and Spradling, 2016; Ikami et al. 2023), contain more Visham. Similar clustering occurs in germline cysts of

Drosophila and many species (see Hegner, 1914; Büning, 1994; Huynh and St Johnston, 2004). Following a cyst division, the bridges migrate over the cell surface to a location close to the cell with the most branches, a process called "rosette formation" (Figure 1H). This morphological change is thought to enhance sharing between nurse cells and oocytes.

Visham is highly enriched in Golgi and vesicles

EMA-1 antisera reacts with multiple fucosylated glycolipids on pre-meiotic germ cells (Apostolopoulos et al. 2015; Figure S1H) and the EMA granule was previously suggested to contain Golgi (Jeon & Kennedy, 1973). Electron microscopy (EM) of mouse germ cells allowed us to identify an oval-shaped region the size of an EMA granule that contained prominent Golgi and endocytic vesicles in most E11.5 and E12.5 cyst germ cells (Figure 1E'; Figure S1K). Visham co-stained with the Golgi protein Gm130 (Figure 1F) and the recycling endosomal protein Rab11a1 (Figure 1F'). Visham often partly overlaps with ER (Figure S1I). Of particular note, in EM sections of E14.5 cysts we found clusters of Golgi within adjacent cyst cells near ring canals as expected for cysts after rosette formation (Figure 1E, 1E"). The particular epitopes recognized by EMA disappear from germ cells at E14.5 (Figure 1I), however, very similar (but non-germ cell-specific) staining with wheat germ agglutinin (WGA) continued in later stages (Figure 1G, G"; Figure S1G)

Visham overlaps centrosomes and moves on microtubules

A cell's microtubule cytoskeleton that emanates from its centrosomes, and from non-centrosomal microtubule organizing centers (ncMTOCs) frequently control trafficking of Golgi elements and position this structure near centrosomes. To investigate the relationship between microtubules and Visham, we stained E11.5 gonads with anti-acetylated-tubulin (AcTub) and EMA. Visham usually overlapped the centrosomes in interphase germ cells (Figure 2A),

indicating it occupies a peri-centriolar domain. In germ cells undergoing mitosis (Figure 2B), Visham associated with centrioles during interphase, but (typical for Golgi) dispersed as a spindle forms and for most of metaphase. In telophase, Visham vesicles gathered at the spindle poles in both daughter cells and at the arrested cytokinesis furrow, which still retained the elongated spindle/midbody microtubules typical of cyst-forming cell cycles (Figure 2B). 3D summary movies of germ cells at these stages stained for AcTub and EMA are shown in Figure S2A).

These behaviors differ from the pattern of Drosophila fusome segregation during cyst divisions (de Cuevas and Spradling, 1998). Visham was rarely seen at just one pole of a spindle like the fusome at very early stages of GSC and cytoblast division; some EMA-reactive material also appeared at the cytokinesis furrow earlier than in the cases of the fusome (Figure 2C; Figure S2C-D). Asymmetry in the Visham distribution later in the cell cycle seemed to arise beginning only in late telophase. Clusters of Visham and centrosomes approached the arrested furrow (Figure 2D, S2C, S2D). At this point short microtubule arrays were visible (Figure 2D, S2C), could be seen. The amount of Visham in the two daughter cells becomes asymmetric, suggesting that differential activity or persistence of Visham transport is important. Ovaries cultured briefly in vitro supported continued germ cell division and Visham asymmetry. Asymmetry was lost if MTs were disrupted by cold or by Celiobrevin D treatment (Figure S2E graph).

Cyst fragmentation is non-random and correlates with microtubule gaps

Mouse cysts produce an average of 4-6 oocytes per PGC as a result of fragmentation (Lei and Spradling, 2013), and gradual reductions of cyst cell numbers and size due to nurse cell activation and turnover (Niu and Spradling, 2022). Cyst breakage may largely be programmed to support production of uniform-sized oocytes (Spradling et al. 2022), but more random

breakage also occurs (Lei and Spradling, 2013; Ikami et al. 2023; Levy et al. 2024). To assess a role of microtubules and Visham in programming cyst fragmentation, we tracked AcTub and Visham in lineage-labeled E12.5 cysts. In about 10% of interphase cysts, presumably those in very late telophase or early in the subsequent cell cycle, persistent microtubule arrays were observed throughout most or all of the cyst that connected the cells in pairs (Figure 2E). When we examined a total of about 50 large cysts, 15 larger cysts of 7-10 cells were found where the MTs in all cells could be analyzed completely. Unexpectedly, all showed a large discontinuity of 10μ or more in microtubule linkage between just two of the 7-10 cystocytes (Figure 2E). Three examples are shown in which projections of 8-cell lineage labeled cysts (green) are outlined (dashed yellow lines). In the left column, Visham is shown in white and MTs in red (Fig. 2E-E"; a 3D movie for 2E is in Figure S2F'). In the middle column, microtubule bundles are seen to connect most cell cells, but are absent between two cells (straight dashed line). The absence of an MT connection predicts cyst fragmentation, as shown in (Figure 2E"), where a separation into a 2-cell and a 6-cell cyst has already occurred.

The predicted patterns of fragmentation were highly non-random (Figure 2F). Production of a 6-cell cysts was strongly preferred based on the position of the gaps (13/15 cysts analyzed). 8-cell or larger cysts all were predicted to generate a subgroup of 6 and whatever additional cell group was left. As discussed below, this preference simply explains the changing pattern of synchronous mitoses observed during E10.5-E14.5 (Pepling and Spradling, 1998), and the consistent ~5-fold increase in the number of accumulated organelles in oocytes in primordial oocytes compared to E14.5 germ cells (Lei and Spradling, 2016).

Visham associates with polarity and microtubule genes including Pard3

Microtubules play a critical role in ovarian cyst formation and polarity in multiple species. Some of the most important regulators of MTs and polarity are the Par proteins that function in epithelial cell polarity, embryonic development, asymmetric neuroblast division (Petronczki and Knoblich, 2001) and oocyte formation in C. elegans, Drosophila and vertebrates (Kemphues et al. 1988; Shulman et al. 2000; Moore and Zernicka-Goetz, 2005). Drosophila meiotic cysts express Baz/Par3 and another apical Par complex protein, Par6, along with beta-catenin/Arm in a ring-like arrangement close to the ring canals (Cox et al. 2001; Huynh et al. 2001). This relatively small membrane zone likely represents the apical domain of cyst germ cells.

We investigated the expression of Pard3, the mouse ortholog of Par3/Baz to determine if a similar arrangement of the highly conserved Par proteins are found in mouse germline cysts, . Pard3 expression localized around Visham but extended beyond it, a pattern reminiscent of the larger ring of Baz in Drosophila cyst cells (Figure 3A, Figure S3A). At E13.5, cysts now in rosette configuration show enriched Pard3 and Visham around the central cell likely to become the oocyte and connecting with lower amounts in more distant cells (Figure 3B, yellow dashed region) but not in E13.5 male cysts (Figure S3B'). This co-localization was validated in lineage labeled E13.5 cysts (Figure 3D; Figure S3D). Visham and Pard3 were located next to ring canals (Figure 3C), demonstrating that mouse cysts have ring canals and an apical Par protein in the same small anterior location as in Drosophila, and that Visham occupies the corresponding zone as the Drosophila fusome.

Visham associates with Golgi genes involved in UPR beginning at the onset of cyst formation

To investigate germ cell gene expression through the entire span of cyst formation and meiotic prophase we carried out new scRNAseq on its earliest stages and combined them with previous data (Niu and Spradling, 2022). We sequenced E10.5, E11.5 and E15.5 fetal germ cells

(see Methods) and added them to data from Niu and Spradling (2022) to make an integrated dataset of more than 3,000 germ cells spanning E10.5 to P5 (Figure 3F-H; Figure S3E-I). Our gene expression studies showed that even PGCs and early cysts actively express genes involved in enhancing the proteome by synthesizing new membrane proteins and expressing high levels of pathways that monitor, refold or expel misfolded or aggregated products for degradation. The UPR pathway associated largely with the ER in yeast is regulated by Hac1, the ortholog of Xbp1. We observed high levels of Xbp1 (Figure 4E) and many of. its targets, genes that can rapidly increase the amount and quality of secretory pathways. Membrane proteins and lipids which are also promoted by this pathway may be in great demand in early germ cells because of the extensive cell proliferation of germ cells, containing diverse membrane proteins and lipids for organelles as well as plasma membranes.

In animals the UPR pathway has been modifed by the addition of several additional pathways besides the Ire1-Xba1 branch. We also observed strong expression Creb3l2 (ER/Golgi resident transcription factor), ATF4 (General UPR transcription factor activated by Golgi stress), Golph3 (Golgi phosphoprotein for membrane trafficking) and Arfgap(s) (involved in both Golgi to ER-and Golgi to endosome trafficking) also showed high expression at E11.5 and during later cyst formation (Fig S3J).

Active Xbp1 activates genes that maintain protein folding, secretion, and cellular adaptation to stress. These include genes involved in misfolded protein expression and refolding such as the chaperones (Hsp5a/Bip, Hsp90b1;DNAjc10; Lman2; Dnajb9), protein-disulfide isomerases (Erp44, Pdia3, Pdia4, Pdia6, Creld2), as well as the ERAD regulator Syvn1/Hrd1 and ERAD components (Sec61b; Ubxn4, Psmc6, Ube2j2, Get4, Ufd1). Thus, repair and expansion of

ER, Golgi and secretory components appears to begin immediately or even before migrating PGCs reach the gonad (Fig 3I).

Xbp1 also supports synthesis of ER membrane phospholipids via upregulation of targets such as Elovl1, Elovl5, and Elovl6, and Chka, Other highly expressed targets including Vcp, Sec61a, Sec63, Surf4, Scrib Lsm14a and Pard1 also maintain ER and Golgi structure and are all orthologs of Drosophila fusome proteins (Figure 3I'). These experiments suggest a significant role for the adaptive UPR pathway and all of its branches during cyst formation. Many of these genes had a second period of expression at the end of meiotic prophase as well (Figure 3I-3I')

Dazl is required for normal cyst formation and UPR.

To investigate the effects of Dazl on cyst formation we confirmed that Dazl$^{-/-}$ mice retard the PGC to germ cell transition (Figure S4C-E). Dazl$^{-/-}$ E12.5 cysts showed higher levels of the DNA methylase Dnmt3a expression compared to controls (Figure 4A; Figure S4A-B) suggesting that they have slowed reductions in germ cell DNA methylation. Ring canals highlighted by staining for Tex14 showed they were only half the size of wild type canals at E13.5 or structurally abnormal (Figure 4B).

We also performed scRNA sequencing of Dazl female homozygous mutant gonad at E11.5 and E12.5 and reclustered them with wild type germ cells at these stages for comparison (Fig 4C). At E11.5 the merged germ cells clustered together suggesting that Dazl$^{-/-}$ has minimal effects on germ cells at E11.5, the stage it is first expressed (Fig 4C). However, E12.5 WT and Dazl$^{-/-}$ germ cells clustered separately (Fig 4C). Wild type and Dazl$^{-/-}$ E11.5 germ cells expressed similar amounts of EGAD mediated UPR pathway genes (Figure S4F) whereas at E12.5 Dazl$^{-/-}$ germ cells expressed higher levels compared to wild type (Fig 4C'). Thus, UPR genes in Dazl$^{-/-}$

cells act similarly to pluripotency genes, and appear to persist at high levels a later development stages than wild type.

The high expression of Xbp1 in PGCs and early cyst cells and many of its target genes argues strongly that early germ cells are expanding ER and Golgi production, and enhancing membrane protein quality. To validate that XBP1 is active in germ cells, we employed an IRE1-XBP1 ratiometric assay which utilizes a genetically encoded dual-fluorescent reporter system (see Methods, Figure S4I). First, we performed magnetic-activated cell sorting (MACS) to purify SSEA1 labelled germ cells from the E11.5 gonad (Figure S4G-H). We delivered the IRE1-XBP1 sensor to SSEA1+ve germ cells and SSEA1-ve control somatic cells by transfection. Both types of cells fluoresce green in proportion to IRE1-splicing activity which measures Xbp1activation activity. The construct also constitutively expresses a red fluorescent marker such that the color ratio will represent a quantitative measure of relative IRE1-XBP1 activity between cells and under different conditions. These observations showed that IRE1-Xbp1 activity in E11.5 germ cells was significantly higher than in somatic cells (Figure 4D). Even higher levels of Xbp1 activity ere seen in Dazl-/- cells (Figure D', D").

The adaptive UPR pathway destroys misfolded proteins using proteasome activity, particularly the 20S proteasome (Vember and Brodsky, 2009; Figure 4H). We measured proteasome activity within E11.5 PGCs to investigate whether the more highly active UPR pathway was paired with increased proteasome activity indicating it likely served an adaptive cellular mechanism of cell rejuvenation in PGCs destined to produce oocytes and their contents. Using a fluorogenic substrate to measure 20S Proteasome activity, we again compared MACS sorted germ cells to somatic cells and found that germ cells have significantly higher proteasome

activity than somatic cells at E11.5 (Fig 4E) and E12.5 (4E', Left Panel). Proteosome activity was even higher in Dazl-/- germ cells (Figure 4E', Right panel and 4E").

We also studied the effects of Dazl mutation on the ability of cysts to acquire asymmetry related to oocyte production as indicated by Visham enrichment in cells with multiple ring canals. Using both EMA and a Golgi marker, Gs28, we observed that germ cell Golgi begin to fragment in *Dazl*$^{-/-}$ mutant germ cells even by E12.5 (Fig 4F, dotted circles). High levels of Golgi stress documented by the increased IRE1-Xbp1 activity, and elevated proteolysis in these cells, may lead to such fragmentation. These problems were accompanied by a dramatic arrest in cyst polarity development. E13.5 in *Dazl*$^{-/-}$ germ cells showed virtually no differential expression of Pard3 or enrichment of Visham with particular cyst cells (Figure 4F'). Finally, analysis showed that in *Dazl*$^{-/-}$ P0 gonads large cells destined by become oocytes do not appear (Figure S5E). The effects of Dazl-/- on germline cyst development and meiosis are summarized in Figure 4G. The observed loss of polarity caused by Dazl mutation can explain the failure of oocyte production and sterility of Dazl homozygotes.

Visham participates in organelle rejuvenation during meiosis

In Drosophila, starting at pachytene the microtubule cytoskeleton is altered in structure, and polarity (Cox and Sprading, 2006). The new polarity, with microtubules running along the fusome such that minus ends cluster in the oocyte, prepares selected nurse cell organelles for transport into the oocyte for inclusion in the Bb of a new primordial follicle Such migration was first described for Drosophila centrioles (Mahowald and Strassheim, 1970). Much later, (Lei and Spradling, 2016; Niu and Sprading, 2022), mouse nurse cell centrosomes, mitochondria, Golgi, ER and possibly other organelles were shown to move between nurse cells and to concentrate in the oocyte between P0 and P4 to the oocyte all move from nurse cells to the oocyte, in a

microtubule-dependent process. Prior to or during these events, Drosophila mitochondria fragment to contain individual genomes, and are selected and rejuvenated by programmed mitophagy to enhance functionality (Lieber et al. 2019; Palozzi et al. 2022; Monteiro et al. 2023). It is not currently known if selection and rejuvenation take place before movement to the oocyte, or if a significant amount also takes place en route.

Because the fusome is directly involved in organelle movement to the Balbiani body in Drosophila post pachytene, we looked for changes in Visham and in gene expression starting at pachytene that might provide further insight into organelle rejuvenation and movement to the oocyte. Visham staining with WGA persists within meiotic germ cells at E17.5 (Figure 5A-A'; Figure S5A,B; S5C Video). Visham volume, remained in proportion with germ cell ring canals, as outer nurse cells (with one ring canal) transfer organelles and cytoplasm to cells with more ring canals located closer to oocytes (Figure 5A graph). Pard3 content also showed such a proportion (Figure 5D). At E18.5, development within germ cells in the ovarian medulla diverged from development in more cortical regions (Figure 5B), as wave 1 that develop without arresting and wave 2 follicles that become quiescent primordial follicles (Yin and Spradling, 2025). Wave 1 oocytes grow substantially in volume, Visham content and Pard3 due to cytoplasmic transfer from surrounding nurse cells which decrease in size (Figure 5B-B' and 5E-E'', Figure S5 E and F, left panel). Oocyte enrichment of Visham and Pard3 was confirmed using lineage labelled cysts at P0 (Fig 5C and 5F). Such enrichment was significantly reduced in Dazl+/- heterozygotes (Figure 5G', G' and Figure S5E and F, middle panel video).

Wave 2 follicles which produce nearly all fertile oocytes, increase organelle content beginning at E18.5 and contain a finished Bb by P4 (Niu and Spradling, 2022). Initially, 4-5 transferred Golgi centrosome pairs were observed at separate cytoplasmic locations in oocytes,

that gradually come together and form an oval-shaped cytocentrum that nucleates a microtubule aster and organizes the Balbinai body. We examined EMs carried out immunofluorescent staining at E18.5 and during this period (Pepling and Spradling, 2001; Pepling et al. 2007) that documented interactions between Golgi, ER and mitochondria (Figure 5H). The left column (H) shows wild type germ cell with a large crescent of perinuclear mitochondria (AT5a, red) adjacent to a large cluster of Visham (WGA, yellow). An EM showing a similar arrangement cluster form an E18.5 germ cells is also shown (Fig 5H'). For comparison in Figure 5H", the same staining of a Dazl+/- heterozygote is shown. The amount of mitochondria is reduced and Visham-staining material is not organized at a hub and appears to be dispersed. In the rightmost column (Figure 5I') ER tracker (cyan) is found is clusters throughout much of the cytoplasm, where EMs consistently show tight interactions between ER plates and mitochondria in almost every part of the cell (5I).

These general observations suggest that during a substantial amount of meiotic prophase, Golgi- and endosome-rich Visham structures in the cytoplasm continue to carry out activities designed to replace, and repurify substantial amounts of the oocyte proteome in every compartment of the cell. Such activities place great demands on the major organelles of the secretory pathway, ER and Golgi, which must synthesize, fold, modify and quality check an enormous number of critically important membrane proteins. High levels of such activity or failure to balance its many interlocking steps can lead to ER and Golgi stress. These activities inevitably generate proteins that failed to fold or recover form aggregation that must be removed and degraded.

DISCUSSION

Early female germ cell development in animals occurs within interconnected cysts formed by consecutive incomplete divisions of a germline stem cell (GSC) or PGC (reviews: King, 1970; Büning, 1994; Pepling et al. 1999; Matova and Cooley, 2001, Hinnant et al. 2020; Spradling, 2023). The identification in mouse cysts of a fusome-like structure, Visham, argues that mechanisms generating cyst polarity on which cyst functions depend have been conserved over the course of animal evolution, even as other properties have changed, such a cyst fragmentation to produce multiple oocytes.

Mouse germline cysts contain a fusome-like structure, Visham, that accumulates preferentially in future oocytes

Our results show that a mammalian analog of the Drosophila fusome does in fact exist which we have termed Visham. The similarities between Visham and the fusome start with its presence as the EMA granule in a small region of the PGC before it arrives at the gonad. The granule transforms into an asymmetric structure during synchronous, incomplete divisions, and passes through structurally similar ring canals. Like the fusome, Visham separates unequally within cyst cells and favors cells with multiple branches that are known to become oocytes. Dividing cysts display stable microtubules using anti-AcTub antibodies that derive at least in part from arrested spindles during incomplete cytokinesis. They persist for only a small part of the cell cycle, yet cyst polarity is maintained, as evidenced by preferential Visham accumulation in future oocytes, and cyst rosette formation. Ongoing Visham polarity is further manifest by its association with the putative apical domain of the cyst germ cells near the ring canals and Pard3, like the Drosophila fusome with Par3 and other conserved apical complex proteins (Huynh et al. 2001). Forming mouse germ cells also express orthologs of many known fusome components

(Figure 3I'). The presence of this conserved polar structure not only supports the conservation of mouse germline cysts during animal evolution, but will be valuable to better understand how germline cysts contribute to early oocyte specification, development and rejuvenation during meiosis and subsequent development.

Many past studies suggest that Golgi-rich structures are relevant to oogenesis in diverse mammals including humans. Large Golgi- associated EMA granules where characterized by EM in E11.5 germ cells (Jeon & Kennedy, 1973). Golgi type membranes forming a large spherical mass in germ cells were reported in classical studies of pig and mouse reproductive tissues (Anderson & Beams, 1960; Clark & Eddy, 1975; Ginsburg et al., 1990). The presence of a fusome like precursor similar to the mouse EMA granule, suggests that development of a fusome-like organelle occurs widely in other mammals. Similar perinuclear structures associated with a Golgi complex in PGCs has been reported in other vertebrate species like chicken and quail (Fazel et al., 1987, 1990; Jung et al., 2005; Urven et al., 1988; Yoshinaga et al., 1991, 1992;Hen et al. 2014).

Significance of potential differences between the Drosophila fusome and Visham

Our findings revealed differences of uncertain significance between Visham and Drosophila fusomes. Visham's major component is Golgi although it associates with ER, including Sec63 (Figure S1H) and Rab11a1 (Figure 1F'), proteins also found in the fusome (Lighthouse et al 2008). In contrast, the fusome contains much of the germ cell's ER, however, Golgi elements are located adjacent to many fusome ER exist sites (Spradling et al 2022). The greatest difference may be the specialized matrix of atypical membrane skeleton proteins within the fusome, a trait currently found only in insects, which gives it stability throughout the cell

cycle, although it ER membranes remain normally connected to other cellular organelles (Snapp et al. 2004).

Differences in Visham compared to the fusome might be due to changes required for PGCs to produce multiple oocytes, something that occurs in many other species and also appears to require cyst breakage (Büning, 1994). However, the non-uniform branching structure and developing polarity of the cyst would seem to require a regulated process of cyst breakage to insure that the smaller cell groups produced would still be able to specify and an oocyte and an appropriate number of nurse cells. The breakage of mouse cysts was discovered activating a GFP lineage marker in E10.5 PGCs that marks the cytoplasm of all subsequent daughter cells (Lei and Spradling, 2013). This powerful approach revealed the outlines of mouse oocyte development from an initial large cyst. However, defining cyst breakage patterns using cytoplasmic GFP is difficult because cytokinesis is prolonged during which cells can move apart and return, requiring a large separation to ensure they have detached irrevocably (20μ according to Levy et al. 2024).

Microtubule patterns predict the location of specific cyst cleavages

We found that the structural properties of cysts prior to the cessation of mitotic divisions at E14.5 can be analyzed by examining their stable microtubules during the period when they can be labeled by AcTub (Figure 2E-F). When visible, smaller cysts had MT arrays that connected all their cells. Surprisingly, the AcTub arrays examined in cysts of 7-10 cells contained a single large gap lacking MTs between a group of 6-cells, and the other two or more residual cells. The conclusion that these gaps predict cleavage sites was suggested by the fact that in some cases they had already visibly separated (Figure 2E"). However, multiple previous observations in vivo provide even stronger support. Synchronous mitoses in forming cysts are distinctive and

easier to map unambiguously than the connectivity of lineage labeled cysts. Based this metric, 6-cell cysts are by far the most commonly observed cyst size not a power of 2 throughout E11.5 to E14.5 (Pepling and Spradling, 1998). Additionally, quantitation of organelles in developing germ cells throughout oogenesis showed that P4 oocytes contained approximately5 times as many centrosomes, Golgi, and mitochondria and four times as much cytoplasm as E14.5 germ cells (Lei and Spradling, 2016). It is difficult to reconcile our results with a model that random breakage due to excess cell movement is a major factor determining cyst size and connectivity (Levy et al. 2024), although it undoubtedly occurs..

Preferential 6:2 cleavage leads to propose a simple model (Figure 5H) for the predominant process by which initial cysts fragment during to generate substrates for meiosis and oocyte development (Figure 2G). 3 synchronous mitotic cell cycles will produce an eight cell cyst with a microtubule gap that fragments to a 2-cell and 6 cell cyst during the ensuing cycle. The next round will produce a 4-cell and a 12 cell cyst, as shown (Figure 2G). After 6-cell mitotic figures, 12-cell synchronous division figures are the second most commonly observed and consistent division pattern not a power of two (Pepling and Spradling, 1998). The one additional postulate needed by the model is that the 12 cell cyst cleaves at its two inner connections to make three 4-cell cysts, which then go on to divide in the final round to make 3 more 8-cell cysts. Combined with another doubling of the 4 four-cell cyst, that will generate 4 eight cell cysts that all cleave to make 6-cell cysts (and 4 2-cell cysts). If all 8-cell cysts have the structure shown, the model predicts an identical structure for all 4 larger cysts, with a central 3-ring canal cell likely to become the oocyte. However, some cleavages may be delayed, and nurse cell dumping sometimes begins even during late cyst formation. Thus, our results suggest that the actual output of most mouse PGCs may be four oocytes. Whether the four two cell cysts produced along side

these larger groups could continue to grow later, or have an alternate function remains to be examined. Other minor pathways of generating a small number of oocytes might also occur.

Many questions regarding cyst formation, fragmentation and oocyte differentiation remain to be answered. How is polarity preserved over the course of cyst formation? How is connectivity disrupted in a controlled way to generate a specific outcome. Because the cleavage arises between two recent cells at one end, it suggests that it was programmed the division before, possibly by one of the outer cells in the 4-cell cyst, possibly the one with very little Visham, an amount that might be insufficient to maintain junction formation. Internal signals, or information from somatic cells which wrap around each ring canal (Pepling and Spradling, 2001) might play a role.. Involvement of the microtubule cytoskeleton in asymmetric divisions has been observed in many situations (Fichelson & Huynh, 2007; Kaltschmidt & Brand, 2002; Sunchu & Cabernard, 2020; Meiring et al., 2020; Planelles-Herrero et al., 2022Watson et al., 2023).

After E14.5, nurse cell transfer becomes a major factor that will change observed cyst sizes by about 1 nurse cell per 6-cell cyst every 2 days, until only the oocyte remains. This must be kept in mind when analyzing previous studies of cyst sizes at different ages.

Early cysts highly expressed genes involved in proteome and secretory pathway remodeling

In animals the UPR pathway has been modified by the addition of several additional pathways besides the Ire1-Xba1 branch, all of which were expressed in early germ cells. Creb3l2 controls a transcription factor that increases production COPII vesicles that carry out ER to Golgi transport and maintain a balance between secretory supply and demand. In sufficient matching can lead to Golgi stress (Machemer, 2015), which can be managed by activating the ATF4 pathway branch.

Expression of Xbp1mRNA or even Xbp1 protein using a general antibody is not sufficient to show Xbp1 activity, since this is controlled by Ire1-mediated splicing to produce the active Xbp1s isoform. We were able to purify enough E11.5 and E12.5 germ cells to carry out biochemical assays and show that mouse female germ cells have substantial levels of Xbp1s activity at both times. Consistent with the likihood that they are enhancing membranes expansion via lipid biosynthesis and throughput of secretory pathways, as well carrying out adaptive-UPR rejuvenation of their proteomes we measured the level of proteolysis in early germ cells as well. Substantial amounts of proteolysis activity were documented at both E11.5 and E12.5

Conserved pre-meiotic germ cell programming in Mouse and Drosophila

Our studies suggested that there are previously unrecognized parallels during early Drosophila and mouse oogenesis between the development of epithelial polarity in germ cells mediated by the Par complex and in secretory pathway activity controlled by the fusome or Visham. Early germ cells express Pard3, Pard6 genes and the Par1 ortholog Mark3 especially in all but the earliest cells (0a, 0b). This mirrors Drosophila findings where the fusome enriches polarity regulators such as Bazooka (Par-3) and Par-1, selectively localized to the oocyte (Cox et al., 2001; Vaccari & Ephrussi, 2002) although only Par3 and Par6 function in oocyte specification (Huynh et al. 2001). In mice, Par-family genes (Pard3, Pard3b, Pard6a/b, Mark3) were previously observed to be downregulated in nurse cells, which was prosed to facilitate cytoplasmic transfer by destabilizing the nurse cell cytoskeleton (Niu & Spradling, 2022; Spradling et al., 2022). Our new scRNAseq further supported these conclusions.

The tight organization of apical Par complex proteins and the ring canals in completed cysts positions the fusome and its Par genes near the edge of the apical region of cell. However,

the function of such a location was never fully clear, despite the fact that loss of either Par3 or Par6 completely blocks oocyte formation, generating instead 16-nurse cell cysts (Cox et al. 2001; Huynh et al. 2001). The potential importance of this localization was highlighted by the finding that a very similar arrangement arises in mouse germline cysts with respect to Pard3. Our finding that Visham is located in the same zone as the fusome in Drosophila, that it is Golgi-rich and that Pard3 is important for Golgi structure (Matsui et al., 2015), provides further evidence that the fusome and Visham produce secretory products during meiosis in developing cysts.

Cysts require DAZL to polarize, accumulate Pard3, and specify oocytes

The function of the RNA binding protein DAZL has been widely studied as a mediator of the PGC to germ cell transition in vertebrates and a regulator of GSC establishment (reviewed in Fu et al. 2015). Dazl is an RNA regulator that affects the post transcriptional processing of many targets and regulates that translation of many others, both positively and negatively. In many organisms it has now been established that during germ cell development translational regulation is especially imporant (reviews: Mercer et al. 2021;). We documented a strong requirement for Dazl early in cyst development. Pluripotency reactivation was blocked since DNA demethylation was arrested, and pluripotency genes failed to shut off at E14.5. The formation of cysts was strongly affected as well, by E12.5. Dazl mutant homozygotes failed generated abnormal ring canals, and failed to normally regulate UPR genes, leaving their mRNA levels elevated. These likely affected the function of these genes and their Xbp1 activator, since both Xbp1 activity and 20S proteosome activity was also elevated in Dazl-/- germ cells. Previously, Dazl had been shown to act as a master translational regulator of mouse spermatogenesis (Li et al. 2019 review) and to arrest oocyte development after diplotene at E18.5. Our studies show that that these and

additional critical functions, including the development of normal cyst with disruption of proper localization of Visham and Pard3.

The act level at which Dazl acts varies in different organisms. Bertho et al. (2024) found that the conserved, germline-specific RNA binding protein Dazl is required in zebrafish to even form stable cysts or to produce oocytes and sperm. In Dazl- incomplete cytokinesis is often abnormal, leading to production of defective ring canals that cannot maintain a stable interconnection or maintain cells in meiosis and produce oocytes. Zagore et al. 2018 acts through polyA -proximal mRNA interactions

The role of ER and Golgi based systems of proteostasis in oocyte development and rejuvenation

Oocytes uniquely bear the burden of repairing all damage suffered by germ cells in the previous life cycle, and restoring its proteome and organelle to the level specified in the genome in order to any limitation to future generations. Meiosis has been shown to restore S. cerevisiae cells when combined with construction of new spores from newly synthesized materials, and population with rejuvented organelles. Meiosis is likely to be the focus of similar rejuvenation in animals. We observed the expression beginning even in PGCs of genes in the UPR pathway. Expression of UPR genes (Figure 3I) was high throughout cyst formation, diminished in leptotene, and then returned during zygotene and eventually reached high levels in diplotene germ cells in which oocyte organelles are interacting with ER and Golgi elements in preparation for organizing into a Balbiani body.

The observations reported here suggest that Golgi- and endosome-associated degradation (EGAD)—an emerging proteostatic mechanism plays a previously unappreciated role. EGAD complements the well-established ER-associated degradation (ERAD) pathway by facilitating the clearance of misfolded proteins via Golgi-endosome trafficking and proteolysis, rather than

removal from the ER and degradation in the proteosome as in ERAD. We observed substantial amounts of ERAD based on the expression of Xbp1 and its many targets, and its documented activity and its endpoint 20S proteosome activity. It is hard to quantitatively compare the amount of EGAD activity, but the prominent role Golgi throughout the stages of mouse oogenesis and its location at the core of the Balbiani body suggests that EGAD either fulfills a unique role in oocyte production. or else is uniquely capable of operating at the highest level of proteostatic activity demanded by the much greater challenge of germline rejuvenation compared to any other tissue without generating damaging and self limiting side effects.

To further dissect the role of Visham-driven UPR signaling in oocyte rejuvenation, we examined Dazl mutant germ cells at multiple times during meiosis. DAZL has been previously been restricting the restored pluripotency of PGCs, a necessary process due to their late specification and previous exposure to mesodermal programming (Gill et al., 2011; Haston et al., 2009; Chen et al., 2014). Dazl is the final part of the return of these cells to a germline fate focused on gamete production (Nicholls et al., 2019) but also in keeping with the use of RNA level regulation in a wide variety of animal gametes whether or not they experience reprogramming.

Dazl has been shown to regulate the expression of a wide variety of genes, including those involved in the ubiquitin-proteasome system, linking it directly to proteostasis control (Fu et al., 2015, Zagore et al., 2018). Our experiments supported the previously documented the importance of Dazl in completing reprogramming, as in mutants DNA methylation was not removed and pluripotency genes were not downregulated. We found that it Dazl$^{-/-}$ germ cells also showed prolonged EGAD-UPR gene expression and sustained high proteasome activity

beyond E11.5, leading to Golgi stress that may have been responsible for fragmented Golgi architecture at E12.5.

Equally damaging to oocyte production was not the loss of cyst formation, as in zebrafish (Bertho et al.) but the loss of polarity as marked by Visham asymmetry. This polarity may have simply been arrested at a very early stage, but regardess, without it subsequent steps need to process cysts, establish groups of nurse cells and a single oocyte, and program the polarity to support future transfers of nurse cell products to the oocyte could not occur and no oocytes were established. By E13.5, failure to specify pro-oocytes becomes apparent, marked by disrupted Visham structure and loss of Par3 polarity enrichment. Even if polarity and oocyte formation had occurred, it is unclear whether the germ cells would have been able to recover and carry out sufficient proteostasis activity to still make a viable oocyte.

Organelle rejuvenation may be regulated by a checkpoint that must be satisfied to move forward, allowing the completion of Golgi assembly into a ring, and consolidation of the Balbiani body structure before the primordial follicle is able to enter a state of cell cycle arrest. A significant level of transcription and translation appears to continue, which would be required to maintain the quality of the organelles and proteome produced be the complex prior period of ovarian development.

MATERIALS AND METHODS

Animals

Mouse strains used-C57BL/6, CAG-cre/ERT2 mice, R26R-EYFP (as described in Lei and Spradling, 2016) and Dazl1L$^{+/-}$ mice (Strain #035880 from JACKSON laboratories). Genotyping was performed according to protocols provided by the JAX Genotyping was performed according to protocols from the JAX Mice database. Animals were provided with a proper light-dark cycle, temperature, humidity, food and water. Sexually mature females and males (6–8 weeks old) were kept for mating. Mating was confirmed through the observation of a vaginal plug. As per standard protocol, we designate the midday of the corresponding day as E0.5, which marks the beginning of embryonic development. Fetal gonads were dissected during E10.5-E18.5 as needed. The day pups are born is designated as P0 and were dissected for some experiments. The Institutional Animal care and use committee of Carnegie Institution of Washington approved procedures for animal handling and experimentation.

Single germ cell lineage labeling

The protocol used for single germ cell lineage labeling was performed as described previously (Lei and Spradling, 2016). Briefly, to obtain fetuses for lineage marking, adult female R26R-EYFP mice were mated with male CAG-cre/ERT2 mice. Tamoxifen was dissolved in corn oil (Sigma) and a single dose was injected intraperitoneally at 0.2 mg per 40 g body weight into pregnant female R26R-EYFP mice at E10.5. Fetal gonads/Pups were dissected as needed in between E11.5-E18.5/P0. To analyze the lineage-labeled germ cells, fixed and frozen whole gonads were subjected to whole mount staining for chicken-GFP, the number of lineage-labeled germ cells of each ovary was determined by examining optically sectioned Z-stack images generated by confocal imaging of the entire ovary.

Immunostaining and quantification

Dissected fetal gonads/ovaries were washed in Phosphate buffer saline (PBS) and fixed immediately in cold 4% paraformaldehyde overnight at 4^0 C. Following the fixation, the gonads were washed three times with $PBST_2$, which is a mixture of phosphate-buffered saline (PBS) with 0.1 % Tween 20 (Sigma) and 0.5 % Triton X (Sigma). Each wash cycle lasted for 30 minutes. Next, gonads were Incubated with primary antibodies mixed with Blocking solution ($PBST_2$+ 10 % Normal donkey serum) overnight at room temperature. Following day, gonads were incubated with fluorescein-conjugated secondary antibodies (Donkey Anti-Rabbit/mouse/rat Alexa-fluor 488/568/647, Invitrogen) overnight at room temperature. Next day, gonads were washed with PBST and stained with DAPI (Sigma) to visualize nuclei. Gonads were mounted on slides with a mounting medium (Vector Labs) and analyzed using confocal microscopy (STELLARIS 8 DIVE Multiphoton Microscope, Leica). Germ cell numbers are quantified in each ovary by manually counting EMA/DDX4 stained germ cells in multiple 0.45 µm optical sections from different ovaries. Details of Antibodies used are provided in SI appendix Table S1.

3D reconstruction and quantification

Three-dimensional model images and movies were generated by Imaris software (Bitplane).For z-stack images, different visualization options in the Surpass mode of Imaris helped to gain visualization control of the objects. To perform surface rendering and volume quantification using Imaris software, we imported your 3D image dataset for EMA/WGA staining. We started with a “Volume” rendering for channels corresponding to EMA/WGA staining and then we adjusted the contrast, brightness and transparency in the “Display Adjustment” window. Next, we used the Surfaces module to create surface renderings by selecting the appropriate

fluorescence channel, applied manual thresholding and adjusted smoothing parameters to define the structure accurately. Once the surface is rendered, we navigated to the statistics tab to access volume measurements. Further visualization of the results was performed in 3D or orthogonal views to confirm accuracy, and adjusted rendering properties such as color or transparency as needed. To create spots for easy counting of labelled cells, we used the "Spots" icon-option in the "Creation" menu and started the spot creation wizard. We set the approximate spot size as per the requirement. Next, we selected the "Manual Creation" option to place spots individually. Each click placed a single spot at the corresponding position.

Sexing and Genotyping

Tail samples from mouse were collected and subjected to lysis and DNA extraction using Proteinase K based lysis buffer treatment at 55^0C overnight followed by 95^0C incubation for 10 minutes. The samples were then centrifuged at 14000 rpm for 5 min to pellet the debris. Extracted genomic DNA from supernatant was used directly and amplified with the Uba1, Sly and Zfy primer pairs for sex determination (McFarlane et al., 2013, Table S2). PCR reactions were performed using KAPA Fast Hotstart ReadyMix with dye (Kappa Biosystems, #KK5608) using the following PCR parameters: initial denaturation at 95 ° C for 5 min, 35 cycles with 94 °C for 30 s, 60° C and 72° C for 30 s, followed by final elongation at 72° C for 5 min. PCR products were analyzed with a DNA ladder (100 bp) on 2% agarose gels and visualized with ethidium bromide under UV-illumination. The male and female amplicon can be distinctly visualized due to different amplicon sizes of PCR products (Table S2).

Electron microscopy

Whole ovaries were dissected in PBS and fixed in 4% Paraformaldehyde overnight. After three 3-min washes in cacodylate buffer, ovaries were postfixed in 1% OsO4, 0.5% K3Fe {CN)6 , in

cacodylate buffer for 1 hour and were rinsed twice for 5 min in cacodylate buffer and once for 5 min with 0.05 M maleate (pH 6.0). The ovaries were stained in 0.5% uranyl acetate overnight at 4 degrees rinsed in water and dehydrated through an ethanol series. Following two 10-rain washes with propylene oxide, the ovaries were infiltrated with resin. The resin-embedded specimen was polymerized by incubation at 45^0 C and 70^0 C for 12 hours each. Silver-gold sections were cut, stained with lead citrate, and observed in the electron microscope.

Single cell RNA sequencing of Wildtype E10.5, E11.5 and E15.5 gonad

Embryonic ovaries were dissected such that individual fetal gonad at E10.5 (18 gonads from 3 females) , E11.5 (12 female gonad from 3 females) and E15.5 (10 gonad from 2 females) were collected. For E10.5 and E11.5: corresponding tail were labelled for identification and placed in 1× PBS on ice. We performed quick Quinacrine and DAPI staining (~15 min) of corresponding E10.5 and E11.5 fetal tail samples to eliminate the male gonad samples -with positive Quinacrine staining of tail samples. We then pooled the dissected female gonad sample and dissociated it into single cells using 0.25% Trypsin at 37^0 C for 5-7 min with two pipet trituration in between. Fetal bovine serum (10 %) was then used to neutralize trypsin. Dissociated cells were passed through 100-µm strainer. The cell suspension was centrifuged at 300 g for 5 minutes and cell pellet was resuspended in freshly prepared and filter-sterilized 0.04% BSA. Viability of cells was assessed via trypan blue staining and >90 percent viable samples were selected and loaded (~10000 live cells for E11.5 and E15.5, ~20000 cells for E10.5) onto the 10X Genomics Chromium Single Cell system using the for E11.5 and E15.5-v3 and for E10.5 v4 chemistry as per the manufacturer's instruction. Single-cell RNA capture and library preparations were performed, and standard data was data processing was performed using Cell ranger pipeline

(6.0.1 – for E11.5 and E15.5 and 8.0.1-for E10.5) and later data was visualized and analyzed by Seurat v5.1.0.

Single cell RNA sequencing of Dazl1L mutant gonad

Dazl+/- female and males were kept for mating and plugged females were marked as E0.5. The gonad from E11.5, E12.5 fetuses were dissected, fetuses were collected in and kept in cold PBS in 12-well plate such that each well with individual fetus is marked for identification. Fetal tails were collected, labelled and subjected to kapa express extract kit (Catalog #KR0383-v4.16) mediated fast DNA extraction according to manufacturer's protocol. Briefly, one step lysis and DNA extraction system was set up in 100 µl volume by adding 10 µl express extract buffer, 2 µl of express extract enzyme and 88 µl of PCR grade water in each tail sample followed by 75^0 C incubation in heating block for 15 minutes for lysis. The samples were then incubated at 95^0C in heating block for 5 minutes for DNA extraction. The sample was then centrifuged briefly to pellet the debris, and supernatant was used directly for PCR as mentioned in methods section of RNA isolation, cDNA synthesis and PCR. The standard genotyping JAX protocol for strain 035880 is referred to identify homozygous / heterozygous and wild type fetuses. Simultanoeusly male/female sexing was also performed (primer details in Table S2). After correct identification, homozygous fetuses-from E11.5 (6 gonad from 3 females) and E12.5 (6 gonad from two females)- were trypsinized to prepare live single cells which were then subjected to 10X Genomics Chromium (v3 chemistry) and data was processed using cell ranger pipeline 6.0.1 and analyzed using seurat v5.1.0 in same manner as mentioned previously for E11.5 gonad.

Cell Identification and Clustering Analysis

Single-cell RNA sequencing (scRNA-seq) data were analyzed using the Seurat package (v5.1.0, https://satijalab.org). Count data generated by the Cell Ranger pipeline (6.0.1/8.0.1) were imported

into R using the Read10X function and converted into a Seurat object with the CreateSeuratObject function. R packages were used to filter out the low-quality cells, and the following criteria were used to filter cells:

a) **for E10.5 WT gonad**: nFeature_RNA > 500 & nFeature_RNA < 8500 & nCount_RNA > 500 & percent.mt < 5

b) **for E11.5 WT gonad**: nFeature_RNA > 100 & nFeature_RNA < 11000 & nCount_RNA > 300 & percent.mt < 10

c) for E15.5 WT ovary: nFeature_RNA > 500 & nFeature_RNA < 9000 & nCount_RNA > 500 & percent.mt < 10.

The filtered count matrices were Log-normalized using the "NormalizeData" function and scaled with the "ScaleData" function to prepare for dimensionality reduction. "Principal Component Analysis (PCA)" was then applied to reduce dimensionality, followed by using top 15 dimensions and default resolution to cluster cells based on gene expression profiles using the "FindNeighbors" and "FindClusters" functions. Cell populations were visualized using the umap method, facilitating the identification of distinct cell types.

Bioinformatic segregation of female germ cells

To segregate E10.5 and E11.5 XX-specific germ cells with complete surety we performed bioinformatic segregation of female germ cells to address the limitations of primitive Quinacrine staining. The expression of the X-linked gene Xist, Ddx3x, Utx etc., were used as a marker. Cells with significant Xist or other X-linked gene expression expression were labeled as "XXonly" using the "Idents" and "WhichCells" R functions. A new Seurat object containing only XX-specific cells was created using the subset function. Germ cells within this subset were identified by examining the expression of germ cell-specific marker genes, and a further subset of E10.5 and E11.5 female germ cells was created using the subset function to focus on germ cells specifically.

Merged dataset creation and Validation

ScRNA-seq datasets from E11.5 to P5 (retrieved from the GEO database, GSE136441 and merged object submiited to Github) were visualized using Seurat. E11.5 cells were discarded and new merged dataset from E10.5-P5 was created, subsets of germ cell clusters from E10.5, E11.5, and E15.5 were integrated using Seurat's "Merge" function. The resulting merged dataset was then processed by normalizing and scaling the data, followed by the identification of variable genes. Th ebatch correction was performed using and pre-harmony and post-harmony data was assessed by visualizing LISI (Local Inverse Simpson's Inde) score confirming successful batch mixing. Cell clusters were determined using Seurat's shared nearest neighbor (SNN) algorithm with PCA reduction using top 15 dimesnions and 2.8 resolution . To visualize these clusters, dimensionality reduction was applied (umap) with following criteria: RunUMAP(new_merge, dims=1:15, n.neighbors = 40, min.dist = 0.6, spread=1) enabling the identification of distinct cell populations.

Cell cycle stages of germ cells across the different developmental stages (E10.5-P5) were validated by visualizing meiosis stage specific expression pattern via feature plot. This visualization technique allows for the capture of subtle trends and helps in comparing expression peaks, providing insights into the transition from mitosis to meiosis across the different developmental stages. Additionally, a violin plot was employed to visualize the variability in average raw UMI levels across germ cells. This approach allowed for an effective comparison of gene expression profiles, highlighting the differences in gene expression patterns between different stages.

Dazl merged dataset

For E11.5 and E12.5 Dazl$^{-/-}$ dataset, cells were filtered based on following criteria:

a) **for E11.5 Dazl -/- ovary** : nFeature_RNA > 500 & nFeature_RNA < 9000 & nCount_RNA > 500 & percent.mt < 5

b) **for E12.5 Dazl-/- ovary** nFeature_RNA > 500 & nFeature_RNA < 10000 & nCount_RNA > 500 & percent.mt < 5

Top 15 dimensions were used at default resolution to cluster the cells which were then visualized by umap. To create merged dataset from subset containing only germ cells were created and merged using "merge" function as described previously. Three dataset were created -for E11.5 wildtype and Dazl$^{-/-}$ dataset, for E12.5 and Dazl-/- dataset and one dataset was created where both E11.5 and 12.5 WT and Dazl-/- were merged. Batch correction was applied using harmony. Merged dataset was normalized, scaled and top 15 dimensions at resolution of 0.4 was used for visualization using umap.

In vitro **gonad culture: microtubule inhibitor treatment and Lysotracker/Mitotracker/ER tracker assay**

To perform in vitro culture of mouse fetal ovaries on membrane inserts with or without inhibitors, we prepared sterile culture medium, constituting DMEM/F-12 supplemented with 10% fetal bovine serum and penicillin-streptomycin. Inhibitor stock solutions were prepared in DMSO and diluted at desired concentration in culture media (Ciliobrevin D from Millipore, 25 μM for 6 hours). Control medium containing the vehicle DMSO was prepared simultaneously. Fetal ovaries were dissected from E11.5 embryos under a stereomicroscope in sterile PBS, we have kept the surrounding mesonephric tissue intact and attached to the gonad to ensure proper development. We have also collected corresponding fetus tail of each fetal gonad to perform genetic sex determination. We have placed membrane inserts into a 24-well plate and added ~500 μL of culture medium (with or without inhibitors) to the lower chamber and ensured no contact between medium and the insert surface. Next, we gently placed isolated ovaries onto the

membrane surface using sterile forceps. The plate is then incubated in a CO_2 incubator at 37°C for ~6 hours. After the designated culture period, confirmed ovaries (post genetic-sex analysis), were carefully removed from the membrane inserts and washed three times with basal media to remove any residual inhibitors. Next, we collected ovaries and fixed in 4% PFA for downstream immunolocalization studies. To inhibit the microtubule growth using cold treatment, we transferred dissected gonad to a chilled culture medium, maintained at 0–4°C. The tissue is fully immersed in the pre-cooled medium and incubated on ice for ~60 minutes. This low-temperature exposure destabilizes microtubules by disrupting tubulin dynamics, effectively depolymerizing existing microtubules and inhibiting further polymerization. After the incubation, the tissue is washed with fresh ice-cold medium and fixed in 4% PFA. To stain specifically for organelles: Fetal ovaries were dissected and cultured in vitro in DMEM/F12 medium supplemented with organelle-specific fluorescent dyes. LysoTracker™ Deep Red (Thermo Fisher, L7528, 1 mM stock) or MitoTracker™ Green (Thermo Fisher, M7514) or MitoTracker™ Deep Red (Thermo Fisher, M22426), and ER-Tracker™ Green (Thermo Fisher, E34251) or ER-Tracker™ Red (Thermo Fisher, E34250) were each added at a final concentration according to the manufacturer's recommendations. The ovaries were incubated in this dye-containing medium at 37 °C with 5% CO_2 for 12 hours. Following incubation, tissues were collected and fixed in 4% paraformaldehyde (PFA) for subsequent immunostaining.

Magnetic activated cell sorting (MACS)

Embryonic ovaries were pooled and treated with Trypsin then were neutralized followed by centrifugation as mentioned before to in ScRNA Sequencing method section to create dissociated single cells. The resulting cell pellet was re-suspended in ~80 microliters MACS buffer i.e. PBS with 0.5% BSA and 2 mM ethylene diaminetetraacetic acid (EDTA). ~20 microliters Anti-

SSEA1 (CD15) microbeads (MiltenyiBiotec Inc., #130-094-530) were added to the cell suspension followed by incubated for 20 min on ice. After adding 1 ml MACS Buffer to the suspension, the SSEA1 bound cells were pelleted by centrifugation at 300 g for 10 min at 4°C. SSEA1+ve and SSEA1-ve cells were then separated by applying cell suspension to MS columns according to the manufacturer's instruction (MiltenyiBiotec Inc.). The SSEA1+ve cells were retained by the column and were filtered thrice to obtain pure germ cell population. The cells were counted, and viability was assessed via trypan blue staining and using automated cell counter (Fischer Scientific). For validation of MACS protocol the cells were fixed in 4 % PFA to perform Immunostaining of DDX4 and were also stored in trizol to perform RNA synthesis and PCR for germ cell specific gene expression.

IRE1-Xbp1 Assay

The IRE1-XBP1 ratiometric assay (from Montana Molecular #U0921G) is a genetically encoded biosensor system utilizes a BacMam Vector carrying dual-fluorescence biosensor. For each assay reaction 50 μl transduction mix consisting of XBP1-IRE1 sensor (15 μl) plus sodium butyrate (0.6 μl per well) was prepared in basal media. To standardize the working conditions, manufacturer provided thapsigargin (1 μm per well) was used as positive control and untransduced cells were used as negative control. For each experiment equal amounts of SSEA1-ve and SSEA1 +ve cells were added to a 96-well plate in duplicates. ~50 microliters of transduction mix was added to each reaction well. The plate was incubated for 45 minutes at room temperature and then transferred to 5% CO2 and 37°C for 24 hrs. The enzymatic activity was then measured at 37°C by monitoring XBP1-IRE-1 sensor's Green fluorescent intensity (top read) at Ex/Em=488/525 nm and basal

constitutive red fluorescent intensity at 565/620 using microplate reader (BioTek Synergy H1).

20S Proteasome activity assay

To perform proteasome activity assay (Amplite #13456) we followed manufacturer's instructions. We first standardized the working conditions using trypsin enzyme as technical positive control. Trypsin is loaded on different well in different concentrations in duplicates. Blank medium along with assay buffer were added in separate wells to act as Negative control. For each experiment equal amounts of SSEA1-ve and SSEA1 +ve cells were added to a 96-well plate in duplicates. ~50 microliters of working solution consisting of fluorogenic substrate in assay buffer (prepared according to manufacturer's instructions) were added and plate was incubated for 2 hours at 37ºC. The enzymatic activity was then measured at 37ºC by monitoring fluorescent intensity (top read) at Ex/Em=490/525 nm (Cut off =515 nm) using microplate reader (BioTek Synergy H1).

RNA isolation and cDNA synthesis

Total RNA was extracted using TRIzol reagent (Invitrogen) following the manufacturer's instructions. Briefly, tissue samples were homogenized in TRIzol, or cells were incubated in TRIzol for 5 min at RT, followed by phase separation with chloroform (200 µl/ml TRIzol, shake for 10-15 seconds and keep at RT for 5 min) and centrifugation at 12,000 × g for 15 minutes at 4°C. The aqueous phase was collected, and RNA was precipitated with equal amount of isopropanol (10 min RT then same centrifugation as last step), washed with 75% ethanol, centrifuged, removed the supernatant ethanol and air-dried. Resuspended pellet in RNase-free water. RNA quality and concentration were determined spectrophotometrically. For cDNA

synthesis we used Superscript IV cells Direct cDNA synthesis kit (Invitrogen, #11750150) with and modified manufacturer's protocol. We skipped the lysis step and directly added DNASe I to our sample (0.5 µl each) followed by 10 minutes incubation on ice. Then we added Stop solution (3 µl each) and kept the mixture at RT for 2 minutes. Then we set up RT reaction as per manufacturer's instruction by adding 8 µl of RT mix to each sample and setting up the following reaction in PCR thermocycler: 25^0 C for 10 min, 55^0 C for 10 min, 85 ^{0} C for 5 min and hold at 4 ^{0} C. cDNA was used directly for PCR as mentioned in Sexing and genotyping using DDX4 and GAPDH Primers (Table S2).

Statistical analysis

Data are presented as mean±SEM (Standard error of mean). Data were analyzed by t-test/one-way Anova. P-value less than 0.05 is denoted by one star. P-value less than 0.01 is denoted by two stars. P-value less than 0.001 is denoted with three stars.

ACKNOWLEDGEMENTS

We thank Wanbao Niu and Mike Sepanski for generating a laboratory archive of EM images of mouse ovaries that was used to prepare Figures 1E and 5H. We thank Wanbao Niu, Qi Yin, and Ashish Tiwari for sharing insights on mouse developmental genetic technology and its application to the ovary. The authors thank Ru-ching Hsia for assistance in electron microscopy including the images of Figures 1E' and S1K. We thank Dr. Eugenia Dikovsky for skillfully managing the Carnegie mouse facility. We thank Allison Pinder and Dr. Frederic Tan for assistance with genomics. Allan Spradling is an Investigator of the Howard Hughes Medical Institute, which provided major support for these studies. We thank members of the Spradling lab for helpful comments throughout the course of the research and publication process. Allan

Spradling is a Staff Member of the Carnegie Institution for Science who hosts the laboratory at its former Department of Embryology, and provides generous additional support.

DATA AVAILABILITY

Raw sequencing data has been deposited at Gene Expression Omnibus (GEO) database (accession: GSE303512). Any additional information required to reanalyze the data reported in this paper is available upon request.

DECLARATION OF INTERESTS

We declare no competing financial interests. One of us (ACS) is an adjunct professor (without compensation) at the Johns Hopkins University Department of Biology and Johns Hopkins University School of Medicine.

REFERENCES

Apostolopoulos, V., Stojanovska, L., & Gargosky, S. E. (2015). MUC1 (CD227): A multi-tasked molecule. Cellular and Molecular Life Sciences, 72, 4475–4500. DOI: https://doi.org/10.1007/S00018-015-2014-Z

Bertho, S., Clapp, M., Banisch, T. U., Bandemer, J., Raz, E., & Marlow, F. L. (2021). Zebrafish dazl regulates cystogenesis and germline stem cell specification during the primordial germ cell to germline stem cell transition. Development, 148. DOI: https://doi.org/10.1242/DEV.187773

Adam Bohnert, K., & Kenyon, C. (2017). A lysosomal switch triggers proteostasis renewal in the immortal C. elegans germ lineage. Nature. *551:7682*, *551*(7682), 629–633. DOI: https://doi.org/10.1038/nature24620

Anderson, E., & Beams, H. W. (1960). Cytological observations on the fine structure of the guinea pig ovary with special reference to the oogonium, primary oocyte and associated follicle cells. Journal of Ultrastructure Research, 3, 432–446. https://doi.org/10.1016/S0022-5320(60)90021-6

Büning J. (1994). The Insect Ovary: Ultrastructure, Previtellogenic Growth and Evolution. Chapman and Hall. DOI: https://doi.org/10.1007/978-94-011-0741-9

Chen, H. H., Welling, M., Bloch, D. B., Muñoz, J., Mientjes, E., Chen, X., Tramp, C., Wu, J., Yabuuchi, A., Chou, Y. F., Buecker, C., Krainer, A., Willemsen, R., Heck, A. J., & Geijsen, N. (2014). DAZL Limits Pluripotency, Differentiation, and Apoptosis in Developing Primordial Germ Cells. Stem Cell Reports, 3, 892. DOI: https://doi.org/10.1016/J.STEMCR.2014.09.003

Clark, J. M., & Eddy, E. M. (1975). Fine structural observations on the origin and associations of primordial germ cells of the mouse. Developmental Biology, 47, 136–155. https://doi.org/10.1016/0012-1606(75)90269-9

Cox, D. N., Seyfried, S. A., Jan, L. Y., & Jan, Y. N. (2001). Bazooka and atypical protein kinase C are required to regulate oocyte differentiation in the Drosophila ovary. Proceedings of the National Academy of Sciences of the United States of America, 98, 14475–14480. DOI: https://doi.org/10.1073/pnas.261565198

Cox, R. T., & Spradling, A. C. (2003). A Balbiani body and the fusome mediate mitochondrial inheritance duringDrosophila oogenesis. Development, 130, 1579–1590. DOI: https://doi.org/10.1242/DEV.00365

Cox, R. T., & Spradling, A. C. (2006). Milton controls the early acquisition of mitochondria by Drosophila oocytes. Development, *133*, 3371–3377. https://doi.org/10.1242/DEV.02514

de Cuevas, M., & Spradling, A. C. (1998). Morphogenesis of the Drosophila fusome and its implications for oocyte specification. Development, 125, 2781–2789. https://doi.org/10.1242/DEV.125.15.2781

Fazel, A. R., Schulte, B. A., & Spicer, S. S. (1990). Glycoconjugate unique to migrating primordial germ cells differs with genera. The Anatomical Record, 228, 177–184. DOI: https://doi.org/10.1002/AR.1092280209.

Fazel, A. R., Schulte, B. A., Thompson, R. P., & Spicer, S. S. (1987). Presence of a unique glycoconjugate on the surface of rat primordial germ cells during migration. Cell Differentiation, 21 199–211. DOI: https://doi.org/10.1016/0045-6039(87)90456-8

Fichelson, P., & Huynh, J. R. (2007). Asymmetric Divisions of Germline Cells. Progress in Molecular and Subcellular Biology, 45, 97–120. https://doi.org/10.1007/978-3-540-69161-7_5.

Floros, V. I., Pyle, A., DIetmann, S., Wei, W., Tang, W. W. C., Irie, N., Payne, B., Capalbo, A., Noli, L., Coxhead, J., Hudson, G., Crosier, M., Strahl, H., Khalaf, Y., Saitou, M., Ilic, D., Surani, M. A., & Chinnery, P. F. (2018). Segregation of mitochondrial DNA heteroplasmy through a developmental genetic bottleneck in human embryos. Nature Cell Biology, 2018 20, 144–151. https://doi.org/10.1038/s41556-017-0017-8

Fu, X. F., Cheng, S. F., Wang, L. Q., Yin, S., de Felici, M., & Shen, W. (2015). DAZ Family Proteins, Key Players for Germ Cell Development. *International Journal of Biological Sciences*, *11*(10), 1226. https://doi.org/10.7150/IJBS.11536

Giardina AG (1901). Origine dell'oocite e delle cellule nutrici nel Dytiscus. Internationale Monatsschrift Fur Anatomie Und Physiologie, 18, 417–484.

Gill, M. E., Hu, Y. C., Lin, Y., & Page, D. C. (2011). Licensing of gametogenesis, dependent on RNA binding protein DAZL, as a gateway to sexual differentiation of fetal germ cells. Proc. Natl. Acad. Sci.108, 7443–7448. https://doi.org/10.1073/pnas.1104501108

Ginsburg, M., Snow, M. H. L., & Mclaren, A. (1990). Primordial germ cells in the mouse embryo during gastrulation. Development, 110, 521–528. DOI: https://doi.org/10.1242/DEV.110.2.521

Gondos, B. (1973). Intercellular Bridges and Mammalian Germ Cell Differentiation. Differentiation 1, 177–182. https://doi.org/10.1111/J.1432-0436.1973.TB00112.X

Hahnel, A. C., & Eddy, E. M. (1987). The distribution of two cell surface determinants of mouse embryonal carcinoma and early embryonic cells. Journal of Reproductive Immunology 10, 89–110. https://doi.org/10.1016/0165-0378(87)90069-6

Hancock, G. v., Wamaitha, S. E., Peretz, L., & Clark, A. T. (2021). Mammalian primordial germ cell specification. Development 148, 189217. DOI: https://doi.org/10.1242/DEV.189217

Haston, K. M., Tung, J. Y., & Reijo Pera, R. A. (2009). Dazl Functions in Maintenance of Pluripotency and Genetic and Epigenetic Programs of Differentiation in Mouse Primordial Germ Cells In Vivo and In Vitro. PLOS ONE 4, e5654. https://doi.org/10.1371/JOURNAL.PONE.0005654

Heasman, J., Quarmby, J., & Wylie, C. C. (1984). The mitochondrial cloud of Xenopus oocytes: The source of germinal granule material. Developmental Biology, *105*(2), 458–469. https://doi.org/10.1016/0012-1606(84)90303-8

Hegner, R. W. (1914). Studies on germ cells. I. The history of the germ cells in insects with special reference to the Keimbahn-determinants. II. The origin and significance of the Keimbahn-determinants in animals. Journal of Morphology, 25, 375–509. DOI: https://doi.org/10.1002/JMOR.1050250302

Hen, G., Friedman-Einat, M., & Sela-Donenfeld, D. (2014). Primordial germ cells in the dorsal mesentery of the chicken embryo demonstrate left-right asymmetry and polarized distribution of the EMA1 epitope. Journal of Anatomy, 224, 556–563. https://doi.org/10.1111/JOA.12163

Hill, J. H., Chen, Z. & Xu, H. (2014) Selective propagation of functional mitochondrial DNA during oogenesis restricts the transmission of a deleterious mitochondrial variant. Nat. Genet. 46, 389–392.

Hinnant, T. D., Merkle, J. A., & Ables, E. T. (2020). Coordinating Proliferation, Polarity, and Cell Fate in the Drosophila Female Germline. Frontiers in Cell and Developmental Biology 8, 19. DOI: https://doi.org/10.3389/FCELL.2020.00019

Huang, Z., Xie, L., Feng, H., Lan, M., Xu, T., Chen, D., Pu, L., & Lu, Y. (2024). DAZL regulate germline, pluripotency, and proliferation related genes in chicken PGCs and cooperate with DDX4. Theriogenology, 222, 22–30. DOI: https://doi.org/10.1016/J.THERIOGENOLOGY.2024.03.010

Huynh, J. R., Shulman, J. M., Benton, R., & St Johnston, D. (2001). PAR-1 is required for the maintenance of oocyte fate in Drosophila. Development, 128, 1201–1209. https://doi.org/10.1242/DEV.128.7.1201

Huynh JR, St Johnston D. (2004). The origin of asymmetry: early polarisation of the Drosophila germline cyst and oocyte. Curr Biol. 14, R438-49. doi: 10.1016/j.cub.2004.05.040.

Ikami, K., Shoffner-Beck, S., Weh, M. T., Schnell, S., Yoshida, S., Miranda, E. A. D., Ko, S., & Lei, L. (2023). Branched germline cysts and female-specific cyst fragmentation facilitate oocyte determination in mice. Proceedings of the National Academy of Sciences of the United States of America, 120. https://doi.org/10.1073/PNAS.2219683120

Jeon, K. W., & Kennedy, J. R. (1973). The primordial germ cells in early mouse embryos: Light and electron microscopic studies. Developmental Biology. 31, 275–284. https://doi.org/10.1016/0012-1606(73)90264-9

Jung, J. G., Kim, D. K., Park, T. S., Lee, S. D., Lim, J. M., & Han, J. Y. (2005). Development of Novel Markers for the Characterization of Chicken Primordial Germ Cells. STEM CELLS 23, 689–698. https://doi.org/10.1634/STEMCELLS.2004-0208

Kaltschmidt, J. A., & Brand, A. H. (2002). Asymmetric cell division: microtubule dynamics and spindle asymmetry. Journal of Cell Science, 115, 2257–2264. DOI: https://doi.org/10.1242/JCS.115.11.2257

Kemphues, K. J., Priess, J. R., Morton, D. G., & Cheng, N. (1988). Identification of genes required for cytoplasmic localization in early C. elegans embryos. Cell, 52, 311–320. DOI: https://doi.org/10.1016/S0092-8674(88)80024-2

King RC. (1970). Oogenesis in Drosophila melanogaster. Academic Press: New York.

King, G. A., Wettstein, R., Varberg, J. M., Chetlapalli, K., Walsh, M. E., Gillet, L. C. J., Hernández-Armenta, C., Beltrao, P., Aebersold, R., Jaspersen, S. L., Matos, J., & Ünal, E. (2023). Meiotic nuclear pore complex remodeling provides key insights into nuclear basket organization. Journal of Cell Biology, 222. DOI: https://doi.org/10.1083/JCB.202204039

Kloc M, Bilinski S, Dougherty MT, Brey EM, Etkin LD. (2004a). Formation, architecture and polarity of female germline cyst in Xenopus. Developmental Biology 266, 43–61. DOI: https://doi.org/10.1016/j.ydbio.2003.10.002.

Kloc, M., Bilinski, S., & Etkin, L. D. (2004). The Balbiani Body and Germ Cell Determinants: 150 Years Later. Current Topics in Developmental Biology, 59, 1–36. DOI: https://doi.org/10.1016/S0070-2153(04)59001-4

Lawson, K. A., Dunn, N. R., Roelen, B. A. J., Zeinstra, L. M., Davis, A. M., Wright, C. V. E., Korving, J. P. W. F. M., & Hogan, B. L. M. (1999). Bmp4 is required for the generation of primordial germ cells in the mouse embryo. Genes and Development, 13(4), 424–436. https://doi.org/10.1101/GAD.13.4.424

Lei L, & Spradling AC. (2013). Female mice lack adult germ-line stem cells but sustain oogenesis using stable primordial follicles. Proc. Natl. Acad. Sci. 110, 8585–8590. DOI: https://doi.org/10.1073/PNAS.1306189110/-/DCSUPPLEMENTAL

Lei L., & Spradling, A. C. (2016). Mouse oocytes differentiate through organelle enrichment from sister cyst germ cells. Science (New York, N.Y.), 352, 95. DOI: https://doi.org/10.1126/SCIENCE.AAD2156

Levy E. W., Leite, I., Joyce, B. W., Shvartsman, S. Y., & Posfai, E. (2024). A tug-of-war between germ cell motility and intercellular bridges controls germline cyst formation in mice. Current Biology 34, 5728-5738. e4. DOI: https://doi.org/10.1016/j.cub.2024.10.062

Lieber, T., Jeedigunta, S. P., Palozzi, J. M., Lehmann, R., & Hurd, T. R. (2019). Mitochondrial fragmentation drives selective removal of deleterious mtDNA in the germline. Nature, 570, 380–384. DOI: https://doi.org/10.1038/s41586-019-1213-4

Lighthouse D, Buszczak M, & Spradling AC. (2008). New components of the Drosophila fusome suggest it plays novel roles in signaling and transport. Developmental Biology 317, 59–71. https://doi.org/10.1016/J.YDBIO.2008.02.009

Lin H, Yue L, & Spradling AC. (1994). The Drosophila fusome, a germline-specific organelle, contains membrane skeletal proteins and functions in cyst formation. Development 120, 947–956. DOI: https://doi.org/10.1242/DEV.120.4.947

Littlefield CL. (1994). Cell-cell interactions and the control of sex determination in hydra. Semin. Dev. Biol.5, 13-20. https://doi.org/10.1006/sedb.1994.1003

Liu, Y., Lau, X., Munusamy, P., Sanchez, C. M. A. S., Snell, D., & Sangrithi, M. (2025). Single-cell RNA-seq identifies protracted mouse germline X chromosome reactivation dynamics directed by a PRC2-dependent mechanism. *Developmental Cell*, *60*(9), 1321-1335.e5.

https://doi.org/10.1016/J.DEVCEL.2024.12.028/ASSET/714FBA10-362A-4CC7-AA61-56D56DC3A471/MAIN.ASSETS/GR4.JPG

Loda, A., Collombet, S., & Heard, E. (2022). Gene regulation in time and space during X-chromosome inactivation. *Nature Reviews Molecular Cell Biology 2022 23:4*, *23*(4), 231–249. https://doi.org/10.1038/s41580-021-00438-7

Machamer, C. E, 2015. The Golgi complex in stress and death. Frontiers in Neuroscience, 9. https://doi.org/10.3389/FNINS.2015.00421

Mahowald, A. P., & Strassheim, J. M. (1970). Intercellular migration of centrioles in the germarium of Drosophila Melanogaster: An electron microscopic study. Journal of Cell Biology, 45, 306–320. DOI: https://doi.org/10.1083/JCB.45.2.306

Marlow, F. L., & Mullins, M. C. (2008). Bucky ball functions in Balbiani body assembly and animal-vegetal polarity in the oocyte and follicle cell layer in zebrafish. *Developmental Biology*, *321*(1), 40–50. https://doi.org/10.1016/j.ydbio.2008.05.557

Matova N, & Cooley L. (2001). Comparative Aspects of Animal Oogenesis. Developmental Biology 231, 291–320. https://doi.org/10.1006/DBIO.2000.0120

Matsui T, Watanabe T, Matsuzawa K, Kakeno M, Okumura N, Sugiyama I, Itoh N, & Kaibuchi K. (2015). PAR3 and aPKC regulate Golgi organization through CLASP2 phosphorylation to generate cell polarity. Molecular Biology of the Cell,26, 751. DOI: https://doi.org/10.1091/MBC.E14-09-1382

Meiring, J. C. M., Shneyer, B. I., & Akhmanova, A. (2020). Generation and regulation of microtubule network asymmetry to drive cell polarity. Current Opinion in Cell Biology 62, 86–95. https://doi.org/10.1016/J.CEB.2019.10.004

Mercer, M., Jang, S., Ni, C., & Buszczak, M. (2021). The Dynamic Regulation of mRNA Translation and Ribosome Biogenesis During Germ Cell Development and Reproductive Aging. Frontiers in Cell and Developmental Biology, 9. DOI: https://doi.org/10.3389/FCELL.2021.710186

Monteiro VL, Safavian D, Vasudevan D, Hurd TR. (2023). Mitochondrial remodelling is essential for female germ cell differentiation and survival. PLoS Genet. 19, e1010610. doi: 10.1371/journal.pgen.1010610.

Moore, C. A., & Zernicka-Goetz, M. (2005). PAR-1 and the microtubule-associated proteins CLASP2 and dynactin-p50 have specific localisation on mouse meiotic and first mitotic spindles. Reproduction, 130, 311–320. DOI: https://doi.org/10.1530/REP.1.00651

Nicholls, P. K., Schorle, H., Naqvi, S., Hu, Y. C., Fan, Y., Carmell, M. A., Dobrinski, I., Watson, A. L., Carlson, D. F., Fahrenkrug, S. C., & Page, D. C. (2019). Mammalian germ cells are determined after PGC colonization of the nascent gonad. Proc. Natl. Acad. Sci. USA, 116, 25677–25687. DOI: https://doi.org/10.1073/pnas.1910733116

Niu, W., & Spradling, A. C. (2020). Two distinct pathways of pregranulosa cell differentiation support follicle formation in the mouse ovary. Proc. Natl. Acad. Sci. USA, 117, 20015–20026. DOI: https://doi.org/10.1073/PNAS.2005570117

Niu, W., & Spradling, A. C. (2022). Mouse oocytes develop in cysts with the help of nurse cells. Cell 185, 2576-2590. e12. https://doi.org/10.1016/J.CELL.2022.05.001

Palozzi, J. M., Jeedigunta, S. P., Minenkova, A. v., Monteiro, V. L., Thompson, Z. S., Lieber, T., & Hurd, T. R. (2022). Mitochondrial DNA quality control in the female germline requires a unique programmed mitophagy. Cell Metabolism, 34, 1809-1823.e6. https://doi.org/10.1016/j.cmet.2022.10.005

Pang, L. Y., DeLuca, S., Zhu, H., Urban, J. M., & Spradling, A. C. (2023). Chromatin and gene expression changes during female Drosophila germline stem cell development illuminate the biology of highly potent stem cells. ELife, 12. DOI: https://doi.org/10.7554/ELIFE.90509

Pepling, M. E., de Cuevas, M., & Spradling, A. C. (1999). Germline cysts: a conserved phase of germ cell development? Trends in Cell Biology 9, 257–262. https://doi.org/10.1016/S0962-8924(99)01594-9

Pepling, M. E., & Spradling, A. C. (1998). Female mouse germ cells form synchronously dividing cysts. Development 125, 3323–3328. https://doi.org/10.1242/DEV.125.17.3323

Pepling, M. E., & Spradling, A. C. (2001). Mouse ovarian germ cell cysts undergo programmed breakdown to form primordial follicles. Dev. Biol., 234(2), 339–351. https://doi.org/10.1006/DBIO.2001.0269

Pepling, M. E., Wilhelm, J. E., O'Hara, A. L., Gephardt, G. W., & Spradling, A. C. (2007). Mouse oocytes within germ cell cysts and primordial follicles contain a Balbiani body. PNAS, *104*(1), 187–192. https://doi.org/10.1073/pnas.0609923104

Petronczki, M., & Knoblich, J. A. (2001). DmPAR-6 directs epithelial polarity and asymetric cell division of neuroblasts in Drosophila. Nature Cell Biol. 3, 43–49. DOI: https://doi.org/10.1038/35050550

Planelles-Herrero, V. J., Bittleston, A., Seum, C., Gaitan, M. G., & Derivery, E. (2022). Elongator stabilizes microtubules to control central spindle asymmetry and polarized trafficking of cell fate determinants. Nature Cell Biol 24, 1606–1616. DOI: https://doi.org/10.1038/s41556-022-01020-9

Reik, W., & Azim Surani, M. (2015). Germline and Pluripotent Stem Cells. Cold Spring Harbor Perspectives in Biology, 7, a019422. DOI: https://doi.org/10.1101/CSHPERSPECT.A019422

Saitou, M., Kagiwada, S., & Kurimoto, K. (2011). Epigenetic reprogramming in mouse pre-implantation development and primordial germ cells. Development, 139(1), 15–31. https://doi.org/10.1242/DEV.050849

Seki Y, Yamaji M, Yabuta Y, Sano M, Shigeta M, Matsui Y, Saga Y, Tachibana M, Shinkai Y, Saitou M. (2007). Cellular dynamics associated with the genome-wide epigenetic reprogramming in migrating primordial germ cells in mice. Development 134:2627–2638. DOI: https://doi.org/10.1242/dev.005611

Suda, Y., Tachikawa, H., Suda, T., Kurokawa, K., Nakano, A., & Irie, K. (2024). Remodeling of the secretory pathway is coordinated with de novo membrane formation in budding yeast gametogenesis. *IScience*, *27*(10). https://doi.org/10.1016/j.isci.2024.110855

Kemphues, K. J., Priess, J. R., Morton, D. G., & Cheng, N. (1988). Identification of genes required for cytoplasmic localization in early C. elegans embryos. *Cell*, *52*(3), 311–320. https://doi.org/10.1016/S0092-8674(88)80024-2

Shulman, J. M., Benton, R., & St Johnston, D. (2000). The Drosophila homolog of C. elegans PAR-1 organizes the oocyte cytoskeleton and directs oskar mRNA localization to the posterior pole. Cell, 101, 377–388. DOI: https://doi.org/10.1016/S0092-8674(00)80848-X

Sekula, M., Tworzydlo, W., & Bilinski, S. M. (2024). Balbiani body of basal insects is potentially involved in multiplication and selective elimination of mitochondria. *Scientific Reports*, *14*(1). DOI: https://doi.org/10.1038/S41598-024-58997-6

Snapp, E. L., Iida, T., Frescas, D., Lippincott-Schwartz, J., & Lilly, M. A. (2004). The Fusome Mediates Intercellular Endoplasmic Reticulum Connectivity in Drosophila Ovarian Cysts. Molecular Biology of the Cell 15, 4512. DOI: https://doi.org/10.1091/MBC.E04-06-0475.

Spradling, A. C., Niu, W., Yin, Q., Pathak, M., & Maurya, B. (2022). Conservation of oocyte development in germline cysts from Drosophila to mouse. ELife, 11. https://doi.org/10.7554/ELIFE.83230

Spradling, A.C. (2023). The ancient origin and function of germline cysts. Results Probl Cell Differ. 71, 3-21. DOI: 10.1007/978-3-031-37936-9.

Suda, Y., Tachikawa, H., Suda, T., Kurokawa, K., Nakano, A., & Irie, K. (2024). Remodeling of the secretory pathway is coordinated with de novo membrane formation in budding yeast gametogenesis. IScience, 27(10). DOI: https://doi.org/10.1016/j.isci.2024.110855

Sunchu, B., & Cabernard, C. (2020). Principles and mechanisms of asymmetric cell division. Development (Cambridge, England) 147, dev167650. DOI: https://doi.org/10.1242/DEV.167650

Unal E, Kinde B, Amon A. (2011). Gametogenesis eliminates age-induced cellular damage and resets life span in yeast. Science 332, 1554–1557.

Urven, L. E., Erickson, C. A., Abbott, U. K., & McCarrey, J. R. (1988). Analysis of germ line development in the chick embryo using an antimouse EC cell antibody. Development, 103, 299-304. https://doi.org/10.1242/DEV.103.2.299

Vaccari, T., & Ephrussi, A. (2002). The fusome and microtubules enrich Par-1 in the oocyte, where it effects polarization in conjunction with Par-3, BicD, Egl, and Dynein. Current Biology, 12, 1524–1528. https://doi.org/10.1016/S0960-9822(02)01079-5.

Vembar, S., Brodsky, J. One step at a time: endoplasmic reticulum-associated degradation. *Nat Rev Mol Cell Biol* **9**, 944–957 (2008). https://doi.org/10.1038/nrm2546

Watson, J. L., Krüger, L. K., Ben-Sasson, A. J., Bittleston, A., Shahbazi, M. N., Planelles-Herrero, V. J., Chambers, J. E., Manton, J. D., Baker, D., & Derivery, E. (2023). Synthetic Par polarity induces cytoskeleton asymmetry in unpolarized mammalian cells. Cell, 186, 4710-4727.e35. https://doi.org/10.1016/J.CELL.2023.08.034

Yamashita, Y. M. (2023). Asymmetric Stem Cell Division and Germline Immortality. *Annual Review of Genetics*, *57*, 181–199. https://doi.org/10.1146/ANNUREV-GENET-022123-040039

Yin, Q., & Spradling, A. C. (2025). Distinct waves of ovarian follicles contribute to mouse oocyte production. BioRxiv, 2024.05.30.596686. DOI: https://doi.org/10.1101/2024.05.30.596686

Yoshinaga, K., Fujimoto, T., Nakamura, M., & Terakura, H. (1992). Selective lectin-binding sites of primordial germ cells in chick and quail embryos. The Anatomical Record 233, 625–632. https://doi.org/10.1002/AR.1092330416

Yoshinaga, K., Muramatsu, H., & Muramatsu, T. (1991). Immunohistochemical localization of the carbohydrate antigen 4C9 in the mouse embryo: a reliable marker of mouse primordial germ cells. Differentiation, 48, 75–82. https://doi.org/10.1111/j.1432-0436.1991.tb00245.x

Zagore, L. L., Sweet, T. J., Hannigan, M. M., Weyn-Vanhentenryck, S. M., Jobava, R., Hatzoglou, M., Zhang, C., & Licatalosi, D. D. (2018). DAZL Regulates Germ Cell Survival through a Network of PolyA-Proximal mRNA Interactions. Cell Reports 25, 1225-1240.e6. DOI: https://doi.org/10.1016/j.celrep.2018.10.012

Figure Legends:

Fig. 1. Mouse pre-meiotic PGCs contain a fusome like structure, "Visham," (A) E9.5-E12.5 ovary stained for EMA and DAPI. White dotted box shown in right panel at higher magnification shows an EMA granule within germ cells (B) E11.5 mouse ovary showing germ cell clone, identified by lineage labelling (YFP, yellow) and germ cell specific (DDX4, green) marker. (B') higher magnification of boxed region showing EMA staining with EMA granule (arrowheads) DAPI, blue. B" a 4-cell cyst clone stained for YFP, DAPI and EMA. Graphs depicting volume within the 3D EMA granule in the 2-cell and 4-cell germ cell clones. Students t- test. Total N=16; 2-cell cyst and N= 18; 4-cell cyst, ***p<0.001. (C) E13.5 ovary (C) and testis (C') stained for germ cell specific GCNA and EMA. Dotted line marks Visham. Graph depicting % germ cells with central branched Visham in E13.5 ovary vs testis. N=26, Student's t-test, ***p<0.001. (D-D') E13.5 germ cell clone stained for EMA, Tex14, and YFP. (D") Visham volume (enriched; >= 10μm^3 , non-enriched;< 10 μm^3) versus ring canal number per cell. N=54. Student's t-test, ***p<0.001. (E-E"). EM images of Visham in E11.5 and E14.5 ovarian germ cells. Dotted red lines mark Visham and red arrows depict Intercellular bridges (IB). (E") is zoomed image from E. (F) E11.5 ovary stained for Gm-130/Rab11a1, EMA and DAPI. Arrows depicts co-localization of Visham with Golgi/Endosomes (G) E11.5 ovary stained for WGA, EMA and DAPI. (G") E13.5 ovary stained for GCNA and WGA. (H) Schematic showing EMA-stained Visham transformation from granule to branched structure. (I) % of germ cells observed with EMA aggregate during E9.5-E14.5. Student t- test. N=15 each (total 90 tissues analyzed), ***p<0.001. Scale bar= 5 μm (A and F'), 10 μm (B-B", C-C', D', F, G-G'), 20 μm (D), 2 μm (E).

Fig 2: Stabilized microtubule and Visham mediate cyst segregation. (A) E11.5 ovary stained for EMA, Pericentrin (PCNT), and DAPI. (A') Schematic depicting Visham colocalization with centrosome. (B) E11.5 gonad stained for EMA, Ac-tub, and DAPI, and schematic (B') depicting Visham behavior during the cell cycle stages. (C) E10.5 gonad stained for EMA, Acetyl. Tub, and DAPI. (C') Schematic depicting that at E10.5, Visham is observed emerging as a spindle remnant. (D) E10.5 Ovary stained for EMA and Ac-tub (D') Schematic depicting Visham's asymmetric separation during cytokinesis (E). Analysis of AcTub and predicted cleave plane of 3 E12.5 cysts (E, E; and E"). Gonad also stained for EMA, and lineage-labelled germ cells (YFP). Right most

panel in each shows putative/confirmed cleavage sites (dashed line) within aeach cyst. (F) Distribution of cell number within predicted cyst cleave fragments. The distribtion differs from . random N=15 lineage labelled cyst (7-cell cyst- 3, 8-cell cyst- 8, 9-cell cyst - 1, 10-cell cyst-3) with clear Ac. Tub connections were analyzed. "A binomial test ($p = 0.253$, one-tailed) showed that '6' was predominant in 13 out of 15 cases, which is statistically significant (****$p < 0.0001$). G) Proposed model of non-random mouse cyst cleavage into 4 6-cell cysts. Scale bar: 5 µm (B) and 10 µm (A, C-E).

Fig. 3. **Localization of Visham in apical cyst region near ring canals, and scRNAseq analysis.** (A-B) E11.5-E13.5 ovary stained for Pard3, EMA, and DAPI. (A'-B') Schematic depicting Pard3 and Visham distribution within E11.5 and E13.5 PGCs (C') E13.5 Ovary stained for Pard3, GCNA and RACGAP (ring canals). (C') Schematic depicting Pard3 enrichment along the cell with multiple ring canals (D) Lineage labelled E13.5 ovary stained for Pard3, GCNA, EMA and YFP. Graph depicting Pard3 versus Visham area quantified via measuring area of staining using Image J. N=13, Student's t-test, ***$p<0.001$. (E) E11.5 mouse gonad stained with Xbp1, EMA and DAPI.(F) 2D-umap plot visualization of merged dataset- E10.5-P5 germ cells- labelled in distinct color depicting developmental stage. (G) Feature plot showing the raw UMI count within different clusters in UMAP plot, dotted line marking the germ cell clusters with low UMI called nurse cells (Nc). (H) Merged dataset categorized by gene marker expression; Pre-meiotic cells (pre-M), Leptotene cells (Lp), Zygotene cells (Zy), Pachytene cells (Pa), Diplotene cells (Dp), Dictyate-arrested (Dc) and corresponding Nurse cells (Nc) (I-I') Stack-violin plot depicting development time course of gene expression of Xbp1 targets across between E10.5-P5. Scale bar:10µm (A-C) and 20 µm (D).

Fig. 4. UPR-proteostasis and cyst polarity regulation is disrupted in Dazl mutants A) E12.5 gonad stained for EMA, Dnmt3a, and DAPI. B) E13.5 gonad stained for Dazl, DAPI and Tex14, and DAPI. Graph showing quantification of ring canal diameter in WT vs Dazl mutant germ cells. N=44, Student's t-test **$p<0.05$ (C) UMAP plot of merged E11.5 and E12.5 WT and $Dazl^{-/-}$ germ cells. (C') Stackviolin plot showing gene expression of Xbp1 and its targets in E12.5 WT vs Dazl mutant germ cells (D-D') IRE1-Xbp1 assay comparing MACS sorted $SSEA1^{+}$ germ vs $SSEA1^{-}$ somatic cells (microscopically in D) at E11.5 across 6 experiments (~32 mice, ≥5 mice and >=20

ovary per experiment. (D”) IRE1-Xbp1 assay comparing SSEA1^{+} vs SSEA1^{-} E12.5 cells in WT or Dazl mutant mouse across 3 experiments (~40 mice, ≥5 mice and >=25 ovary per experiments (E) Proteasome activity in MACS-sorted SSEA1^{+} vs SSEA1^{-} cells using 3 biological assays with ~35–60 E11.5 ovary per assay. (E’) Proteasome activity ratio of MACS-sorted SSEA1^{+} and SSEA1^{-} cells compared at E12.5 and activity ratio of SSEA1^{+ve} and SSEA1^{-ve} E12.5 Wt and Dazl-/- mouse is plotted in E”; ~25–28 E12.5 ovary used per assay. (F) E12.5 WT and Dazl$^{-/-}$ ovary stained for EMA, Golgi marker GS28, and DAPI. (F’) E13.5 WT and Dazl$^{-/-}$ ovary stained for EMA, PARD3 and DAPI. (G) Schematic showing effect of Dazl mutation on premeiotic germ cells (H) Schematic: Visham promotes ERAD-EGAD-UPR-mediated rejuvenation. Scale bar: 10 µm in all except in B-Zoomed in -2µm.

Fig. 5. Visham and Pard3 associate with ER and mitochondria prior to Balbiani body formation (A-A’) E17.5 ovary stained for WGA, GCNA, and Tex14; dotted line shows WGA aggregate with one/two/three ring canals. Graph: Visham volume vs ring canal number. N=65. One-way ANOVA, *p<0.1, ***p<0.001. (B-B’) E18.5 ovary stained for WGA, GCNA and DAPI. Yellow line: medulla/cortex boundary (in B); yellow dotted circle: large medullary oocytes; white dotted area: small nurse cells (in B’). Graph: Visham volume in large (≥15 µm) vs small (<12 µm) germ cells. N=54. Student’s t-test, **p<0.01. (C) Single cell lineage-labelled E18.5 ovary stained for DAPI, YFP, GCNA and WGA. Graph: Visham volume in large (≥15 µm) vs small (<12 µm) lineage labelled cells. N=10. Student’s t-test, ****p<0.0001. (D) E17.5 ovary stained for PARD3, GCNA, RACGAP and WGA; dotted line shows PARD3/WGA aggregate with one/three ring canals. (E) E18.5 ovary stained for DAPI, GCNA and PARD3. Yellow line: medulla/cortex boundary; yellow dotted circle: large medullary oocytes; white dotted area: small nurse cells. (E’) depicts zoomed in image of Oocyte from E’ stained for WGA, GCNA and PARD3. Arrow marks the WGA aggregate and dotted line marks PARD3 stained region. (F) Single cell lineage-labelled E18.5 ovary stained for YFP, GCNA and PARD3. Graph: PARD3 stained area in large (≥15 µm) vs small (<12 µm) germ cells. N=10. Student’s t-test, ****p<0.0001. (G-G’) Dazl$^{+/-}$ mutant stained for WGA, PARD3 and GCNA. Graph: Visham volume in big medullary cells in WT vs Dazl$^{+/-}$. (H) E18.5 WT ovary stained for WGA, ATP5a and GCNA. (H’) EM images depicting Golgi

(arrow) -rich structure surrounded by Mitochondria within E18.5 germ cells. (H”) E18.5 Dazl$^{+/-}$ stained for WGA ATP5a and GCNA. (I) EM images of E18.5 depicting Mitochondria wrapped in ER-exit derived tubule (arrow) like structure. (I’) E18.5 WT ovary stained for ER and Mitochondria tracker plus GCNA. Scale bar: 20 µm (A-A’, B, C-C’, D-D’,E, F-F’, G-G’, H,H” and I’), 5 µm (B’, E’ and E”), 0.5 µm (EM images H’ and I).

SUPPLEMENTARY MATERIALS

Supplementary Tables

Table S1 Materials

Antibody/Lectin/Stains	Company	Catalogue #
EMA	DSHB	EMA-1 AB_531885
GCNA	Abcam	ab82527
DDX4	Abcam/R&D systems	ab13840 & ab27591/ AF2030
SSEA1	DSHB	MC-480
WGA	Thermo Fisher	W7024
Gm-130	ThermoFisher/Novus Biologicals	610822/NBP2-53420
Rab9	Thermo Fisher	MA5-31997
Rab11a1	Thermo Fisher	700184
Tex14	Proteintech	18351-AP
GFP/YFP	Aves Labs	GFP-1020
Dazl	BioRad Labs/GeneTex	MCA2336/GTX89448
Lysotracker deep red	Thermo Fisher	L7528
Pard3	Novus Biologicals	NBP1-88861
LAMP1	Cell Signaling Technology	9091T
Xbp1	Abcam	ab37152
Gs28	BD biosciences	61184
AAL	Vector Labs Inc	FL-1391-1
LCA	Vector Labs Inc	FL-1041-5
Sec63	Thermo Fisher	PA5-100180
Calnexin	Abcam	ab219644
Gs28	Proteintech	16106-1-AP
Acetyl-α-Tubulin (Lys40)	Cell Signaling. Tech	5335S
Alpha Tubulin (acetyl K40)	Abcam	ab289875
Pericentrin	Abcam	ab4448/ab28144
Anti-GCNA1 antibody	Abcam	ab82527
Rac GAP1 Antibody (A-6)	Santa Cruz Biotechnology, Inc	sc-271110
Dnmt3a	Cell Signaling. Tech	3598T
ATP5A	Abcam	ab14748
Mitotracker Green/Deepred	Thermo Fischer	M7514/ M22426
ER-Tracker™ Green/Red	Thermo Fischer	E34251/ E34250
Quinacrine dihydrochloride	Sigma chemical	Q3251

Primer Name	Sequence	Amplicon Size and Reference
Uba1_Forward	5´-TGGTCTGGACCCAAACGCTGTCCACA-3´	Male- 198 bp Female- 217 bp *McFarlane et al., 2013* *(https://doi.org/10.1159/000348677)*
Uba1_Reverse	5´-GGCAGCAGCCATCACATAATCCAGATG-3´,	
Sly_Forward	5'-GATGATTTGAGTGGAAATGTGAGGTA-3'	Male- 280 bp Female- 685 and 480 bp *McFarlane et al., 2013* *(https://doi.org/10.1159/000348677)*
Sly_Reverse	5'-CTTATGTTTATAGGCATGCACCATGTA-3'	
Zfy_Forward	5'-GACTAGACATGTCTTAACATCTGTCC-3'	Male- 180 bp *McFarlane et al., 2013* *(https://doi.org/10.1159/000348677)*
Zfy_Reverse	5'-CCTATTGCATGGACTGCAGCTTATG-3'	
DDX4 Forward	5'-GAGATTGCCTTCAGTACCTATGTG-3'	105 bp *Gao et al., 2011* *(https://doi.org/10.1095/biolreprod.110.084590)*
DDX4 Reverse	5'-GTGCTTGCCCTGGTAATTCT-3'	
GAPDH Forward	5'-GGTGAAGCAGGCATCTGAGGG-3'	246 bp *Chunmei et al., 2011* *(https://doi.org/10.1093/glycob/cwq152)*
GAPDH Reverse	5'-GGTGGGTGGTCCAGGGTT-3'	
Dazl Common	5'-GAC ATT ACT AAG AAA ACA GCA GTG G-3'	Mutant = ~300 bp, Heterozygote = ~300 bp and 192 bp, Wild type = 192 bp *JAX Protocol (Strain #035880, Primer# 56340, 56341 and 56342)*
Dazl WT reverse	5'-TTC TGC ACA TCC ACG TCA TT-3'	
Dazl Mut Reverse	5'-ATC CCT CCC TTT AGG GCT CA-3'	

Table S2. Primers

SUPPLEMENTARY REFERENCES

McFarlane, L., Truong, V., Palmer, J. S., & Wilhelm, D. (2013). Novel PCR Assay for Determining the Genetic Sex of Mice. *Sexual Development*, *7*(4), 207–211. https://doi.org/10.1159/000348677

Gao, L., Kim, Y., Kim, B., Lofgren, S. M., Schultz-Norton, J. R., Nardulli, A. M., Heckert, L. L., & Jorgensen, J. S. (2011). Two Regions Within the Proximal Steroidogenic Factor 1 Promoter Drive Somatic Cell-Specific Activity in Developing Gonads of the Female Mouse. *Biology of Reproduction*, *84*(3), 422–434. https://doi.org/10.1095/BIOLREPROD.110.084590

Chunmei, W., Huang, C., Gu, Y., Zhou, Y., Zhu, Z., & Zhang, Y. (2011). Biosynthesis and distribution of Lewis X- and Lewis Y-containing glycoproteins in the murine male reproductive system. *Glycobiology*, *21*(2), 225–234. https://doi.org/10.1093/GLYCOB/CWQ152

Supplementary Video Link and legends:
Here is the link to Videos use in supplementary figures:
https://drive.google.com/open?id=1XuOoesa_WKMJUaVTpOKGbWWhn_fJc56M&usp=drive_fs

Supplementary Video legends

Video S1A: E13.5 ovarystained GCNA in Green and EMA in Red

Video S1B: E12.5 ovary stained with YFP in Green, EMA in Red, DAPI in Blue

Video S1D1: E13.5 ovary stained for GCNA in Green, DAPI in Blue and EMA in Red

Video S1D2: E13.5 ovary, same region as S3D1 stained for GCNA in Green, and EMA in Red

Video S2A1-S2A5: E11.5 gonadal tissue stained for EMA in Red, Ac. Tub. In Green and DAPI in Blue

Video S2F: 3D modelling of Visham in lineage labelled cyst: YFP in Green, EMA in White and Ac. Tub in Red. Green spheres are spots generated using Imaris software to count lineage labelled cells and Grey surface rendering was performed to visualize the EMA volume.

Video S3A: E13.5 Ovary stained for PARD3 in Red, EMA in Green and DAPI in Blue.

Video S3B1: E1.5 Ovary stained for GCNA in Blue, PARD3 in Red and EMA in Green

Video S3B1: E1.5 Testis stained for GCNA in Blue, PARD3 in Red and EMA in Green

Video S5C: 3D surface rendering of WGA in Red enriched within region spanning ring canal stained by Tex14 in Yellow and GCNA stained germ cells are shown in Green

Video S5D: E18.5 Ovary stained of WGA in Red, GCNA in Green and DAPI in Blue

Video S5 E1-E3: E18.5 Wildtype (E1), Dazl +/- (E2) and Dazl -/- (E3) stained for GCNA in Green and WGA in Red

Video S5 F1-F3: P0 Wildtype (F1), Dazl +/- (F2) and Dazl -/- (F3) stained for GCNA in Green and PARD3 in Red

SUPPLEMENTARY FIGURE LEGENDS

Fig. S1: **EMA/Lectin-stained aggregate (Visham) distribution in pre-meiotic PGCs** (A) Immunostaining of E9.5-E12.5 ovary for germ cell specific marker EMA and DAPI (blue) and for E13.5 ovary (GCNA in green, Z-stack video see Video S1A). (B) Z-stack video of E12.5 ovary stained for EMA, DAPI and lineage labelling shown via YFP (See Video S1B) (C) Volume rendering of EMA aggregate (White arrows) using Imaris software. (D-D') Videos of at E13.5 ovary stained for EMA, GCNA and DAPI (see Video S1D1 and S1D2) (E) Randome 3-D sampling using Imaris for E13.5 ovary showing branched Visham structure within GCNA labelled female germ cells. (F) Images of different E13.5 ovary stained for EMA, GCNA, Tex14 and DAPI. Central region with enriched Visham is often associated with higher number of ring canals. (G) E11.5 ovary stained for WGA, GCNA and YFP as lineage labelling marker. Dotted line marks the WGA aggregate within germ cells. (G') E13.5 ovary stained for WGA, GCNA and Tex14 forming branched WGA-stained Visham structure (dotted lines). **(**H and H') E11.5 gonad stained for general fucosylation specific lectins, AAL/LCA, DAPI and Visham marker EMA. (I and I') Localization of ER markers in vicinity to Visham is validated by staining ER-specific Sec63 or Calnexin, DAPI and EMA. (K) Electron microscopy of E11.5 gonad depicting Golgi clusters (Dotted red lines, labelled as Visham) near intercellular bridges (IB marked by red solid arrows). Scale bar. 100 µm (A), 20 µm (B), 10 µm (in D-H).

Fig. S2. **Validating microtubule dependent Visham formation and its distribution during cyst fragmentation.** (A) Z-stack videos for images used in figure 3A (See Videos from S2A1 to S2A5). (B) E11.5-E12.5 ovary stained for EMA, Pericentrin and Ac. Tub. Arrows mark duplicated centrosome during Interphase. Dotted circles mark centrosomes. Smooth line marks the DAPI stained region during Anaphase depicting clear separation of Nuclei. (C) E10.5 gonad stained for EMA and Ac. Tub. Dotted line marks the newly formed fusome as spindle remnant. (D) Visham asymmetry during cytokinesis depicted in E11.5 ovary stained for EMA (E) In-vitro cultured untreated gonad and treated gonad (microtubule inhibitor Ciliobrevin D and cold treatment)

stained for Ac. Tub, EMA and DAPI. Quantification showing % germ cells with Visham in Untreated versus Celioberivin D/Cold treated E11.5 gonad. (F) Lineage labelled 4-cell cyst stained at E12.5 for YFP , EMA and Ac. Tub. (F') 3D modelling of lineage labelled cyst at E12.5. Video depicts animation video generated using Imaris software to create uniform spheres in green to position the labelled 8-cells within cyst and surface rendering of Visham in White within lineage labelled germ cells (See Video S2F). Scale bar: 5 µm (A-B), 10 µm (C-F).

Fig. S3: Pard3 gene expression in E12.5-E13.5 gonad (A) Z-stack video of E12.5 gonad stained for GCNA, EMA and PARD3 (See Video S3A). (B) Z-stack video of E13.5 ovary **(♀)** and E13.5 testis **(♂)** stained for EMA, PARD3 and GCNA. (C) E13.5 ovary (See Video S3B1) and testis (See Video S3B2) stained for GCNA, EMA and PARD3. (D) Lineage labelled E13.5 ovary stained for YFP, GCNA, PARD3 and EMA. (E) Quinacrine (Male chromosome specific stain) staining of male vs female fetal tail samples (F) Feature plot and UMAP plot depicting Xist expression within E10.5 and E11.5 gonad followed by bioinformatic segregation of female gonadal germ cells (XX only) to avoid Quinacrine false-negative by segregating the cells expressing significant amount of XX specific genes (eg: Xist, Ddx3x, Utx) depicted in UMAP plot as XX only cells. (G) Cluster of germ cells from E12, E14, E16, E18, P1 and P5 of previously published data (NCBI: Niu and Spradling, 2020) were used. E10 (20X genomics), E11 and E15 (10X genomics) ScRNA seq was performed and germ cells isolated bioinformatically to create E10.5-P5 merged germ cell data to comprehensively look at gene expression across developmental stages. The number of cells used to create merged dataset is shown. (H) Feature plot validating all the cells express germ cell specific markers (Dppa3/DDx4) (I) Pre-meiotic/Meiotic gene expression analysis depicted by feature plot for various developmental stages within merged dataset. (J) Stack violin plot depicting Golgi-UPR pathway associated gene expression pattern across E10.5 to P5 meiotic germ cell and nurse cell developmental stages. Scale bar= 20 µm (A,B-B, D) and 10 µm (C), 100 µm (E).

Fig. S4: Validation of female Dazl mutant phenotype, MACS and Activity assays. (A) Expected absence of Dazl protein in Dazl mutant gonad is shown by staining of E18.5 WT and Dazl-/- gonad for Dazl, GCNA and DAPI. (B) E12.5 WT and Dazl$^{-/-}$ gonad stained for DNMT3a, EMA and DAPI (C) Fetal tail genotyping for ScRNA sequencing: Gel electrophoresis showing the standard *Dazl* genotyping PCR assay by Jackson (Stock No: 035880 Protocol 40585) with expected results: Wild type (192 bp), Heterozygous mutant (300 and 192 bp) and Homozygous

mutant (300 bp). (D) Feature plot depicting positive Xist Expression in ScRNA seq data of E11.5 and E12.5 Dazl mutant fetal gonad, thus concluding them as female samples. 8 Dazl $^{-/-}$ fetal gonadal samples from 4 fetal females were obtained for each E11.5 and E12.5 ScRNA seq experiments. (E) Stackviolin Plot depicting pluripotency gene expression pattern in E1.5-E12.5 WT vs Dazl-/- gonad. (F) Stackviolin Plot depicting Xbp1 targets gene expression pattern in E1.5 WT vs Dazl-/- gonad (G) Staining of both unbound SSEA1(-ve) and the bound fraction consisting of SSEA1(+ve) cells for DDX4 and DAPI. (H) Gel electrophoresis showing the PCR amplification of housekeeping gene GAPDH and Germ cell specific marker DDX4 in SSEA1(-ve) and SSEA1 (+ve) germ cells from E11.5 and E12.5 ovary. The amplicon size is indicated on left. (I) Proof of functioning of Xbp1 assay is shown by staining of both mixture of SSEA1(-ve) and SSEA1(+ve) cells for GCNA, DAPI and Red (Xbp1 fluorescence) (J) Proof of function of proteasome activity assay using Trypsin as technical positive control. The proteasome activity assay was shown for two different assays (I and II) with technical duplicates at three different Trypsin concentrations. Mean fluorescent intensity in arbitrary units is shown obtained using plate reader. Scale bar: 20 µm (A), 10 µm (B), 100 µm (G and I).

Fig. S5: Visham enrichment within destined medullary Oocytes in WT vs Dazl mutant. (A-B) Zoomed out E17.5 ovary covering large span of tissue stained with DAPI, WGA, GCNA and Tex14. White dotted line is zoomed in and shown separately in main figure (Refer to main Fig 5A and A'). (C) Video created using Imari software showing E17.5 ovary stained for GCNA, Tex14 and WGA followed by surface rendering of WGA aggregate (continuous one) associated with ring canals. (See Video S5C) (D) Video of E18.5 female gonad stained with DAPI, GCNA and WGA depicts the cortex and medullary region where medullary region showing distinct enriched WGA aggregate compared to surrounding small nurse cells. (See Video S5D) (D') One of the z-stack form E18.5 ovary Video in E stained with DAPI, GCNA and WGA depicts the medullary big Oocyte-like cells showing distinct enriched WGA aggregate compared to surrounding small nurse cells. E) Z-stack video of E18.5 WT, Dazl +/- and Dazl-/- gonad stained for GCNA and WGA. (See Videos S5E1 to S5E3) (F) Z-stack video of P0 WT, Dazl +/- and Dazl-/- gonad stained for GCNA and PARD3. (See S5 F1 to F3) (G) E18.5 WT and Dazl +/- gonad stained for Mitotracker and GCNA. Scale bar: 20 µm (A-B and G), 50 µm (D-E), 100 µm (F).

Fig 1

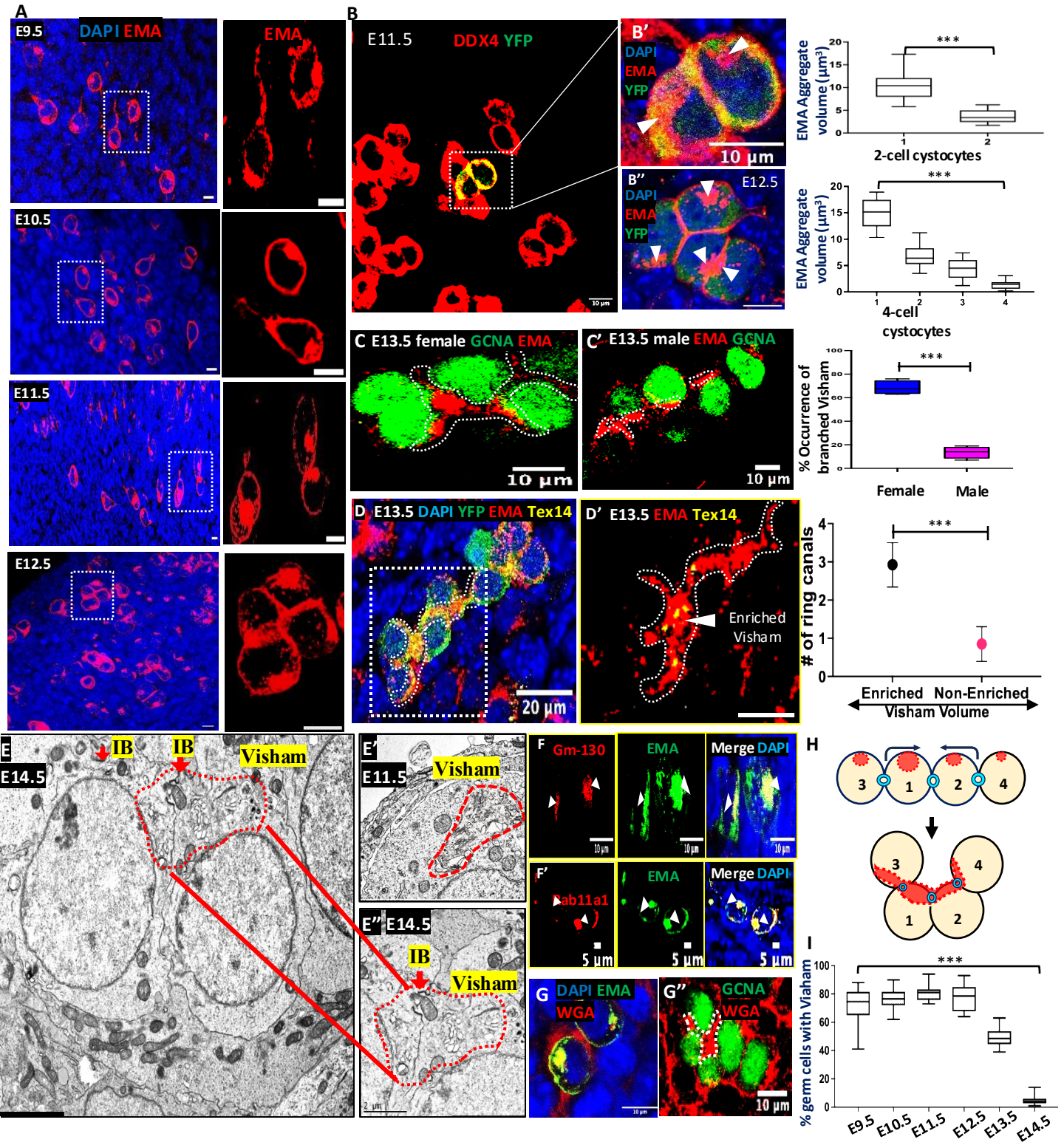
A
E9.5
DAPI EMA
EMA
E10.5
E11.5
E12.5
B
E11.5
DDX4 YFP
B'
DAPI
EMA
YFP
10 µm
B''
E12.5
C E13.5 female GCNA EMA
C' E13.5 male EMA GCNA
10 µm
D E13.5 DAPI YFP EMA Tex14
20 µm
D' E13.5 EMA Tex14
Enriched Visham
E
E14.5
IB
Visham
E'
E11.5
E''
E14.5
F Gm-130
EMA
Merge DAPI
F' ab11a1
5 µm
G DAPI EMA WGA
G'' GCNA WGA
EMA Aggregate volume (µm³)
2-cell cystocytes
4-cell cystocytes
% Occurrence of branched Visham
Female
Male
# of ring canals
Enriched
Non-Enriched
Visham Volume
H
I
% germ cells with Viaham
E9.5
E10.5
E11.5
E12.5
E13.5
E14.5

Fig 2

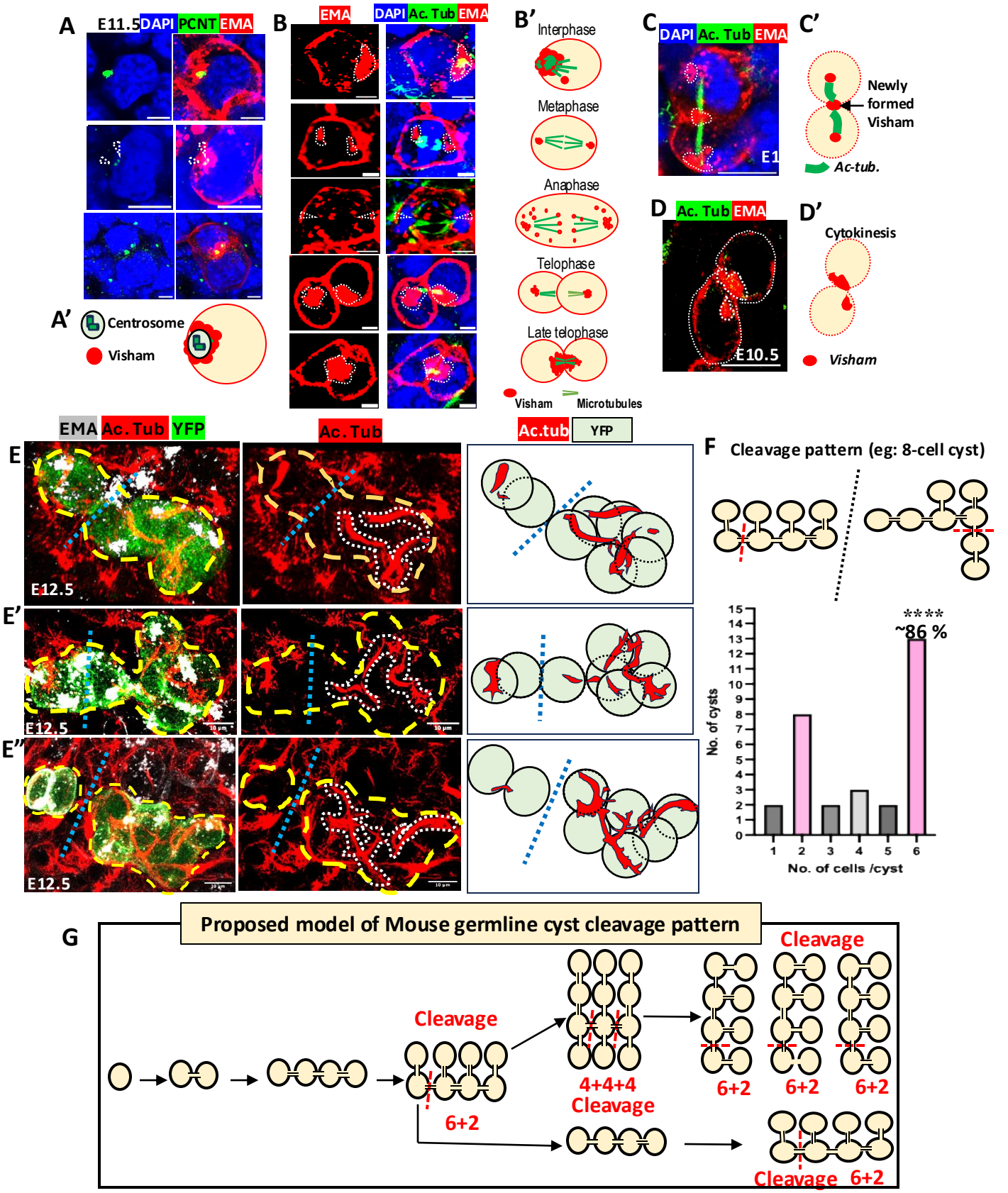
A
E11.5
DAPI
PCNT
EMA
A'
Centrosome
Visham
B
EMA
DAPI
Ac. Tub
EMA
B'
Interphase
Metaphase
Anaphase
Telophase
Late telophase
Visham
Microtubules
C
DAPI
Ac. Tub
EMA
E1
C'
Newly formed Visham
Ac-tub.
D
Ac. Tub
EMA
E10.5
D'
Cytokinesis
Visham
EMA
Ac. Tub
YFP
E
E12.5
E'
E12.5
E''
E12.5
Ac. Tub
Ac.tub
YFP
F
Cleavage pattern (eg: 8-cell cyst)
****
~86 %
No. of cysts
No. of cells /cyst
G
Proposed model of Mouse germline cyst cleavage pattern
Cleavage
6+2
4+4+4
Cleavage
6+2
Cleavage
6+2
6+2
Cleavage
6+2

Fig 3

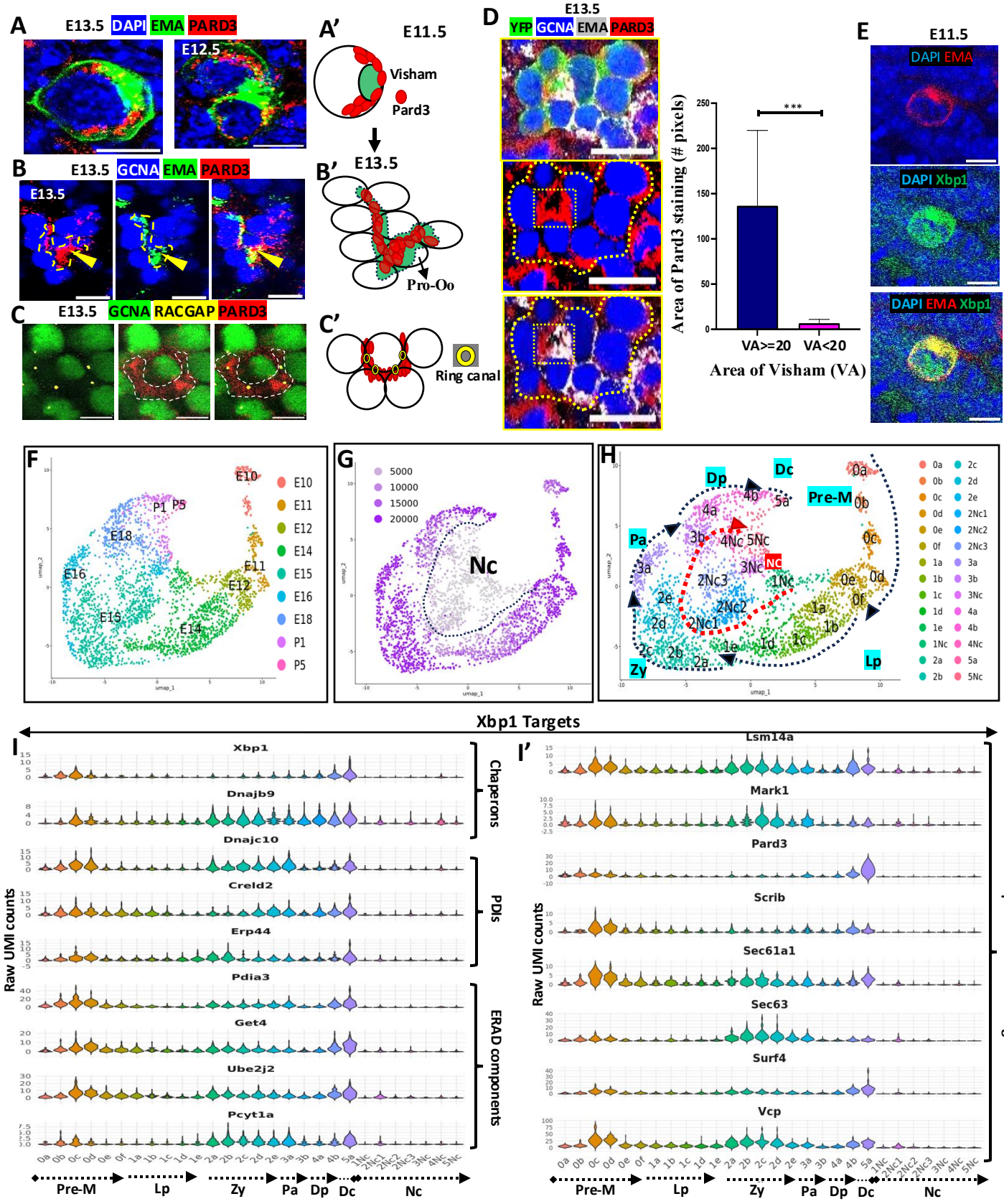
A
E13.5 DAPI EMA PARD3
E12.5
A'
E11.5
Visham
Pard3
B
E13.5 GCNA EMA PARD3
E13.5
B'
E13.5
Pro-Oo
C
E13.5 GCNA RACGAP PARD3
C'
Ring canal
D
E13.5
YFP GCNA EMA PARD3
Area of Pard3 staining (# pixels)
***
VA>=20 VA<20
Area of Visham (VA)
E
E11.5
DAPI EMA
DAPI Xbp1
DAPI EMA Xbp1
F
E10
E11
E12
E14
E15
E16
E18
P1
P5
G
5000
10000
15000
20000
Nc
H
Dp
Dc
Pre-M
Pa
Zy
Lp
NC
Xbp1 Targets
I
Xbp1
Dnajb9
Dnajc10
Creld2
Erp44
Pdia3
Get4
Ube2j2
Pcyt1a
Chaperons
PDIs
ERAD components
Raw UMI counts
Pre-M
Lp
Zy
Pa
Dp
Dc
Nc
I'
Lsm14a
Mark1
Pard3
Scrib
Sec61a1
Sec63
Surf4
Vcp

Fig 4.

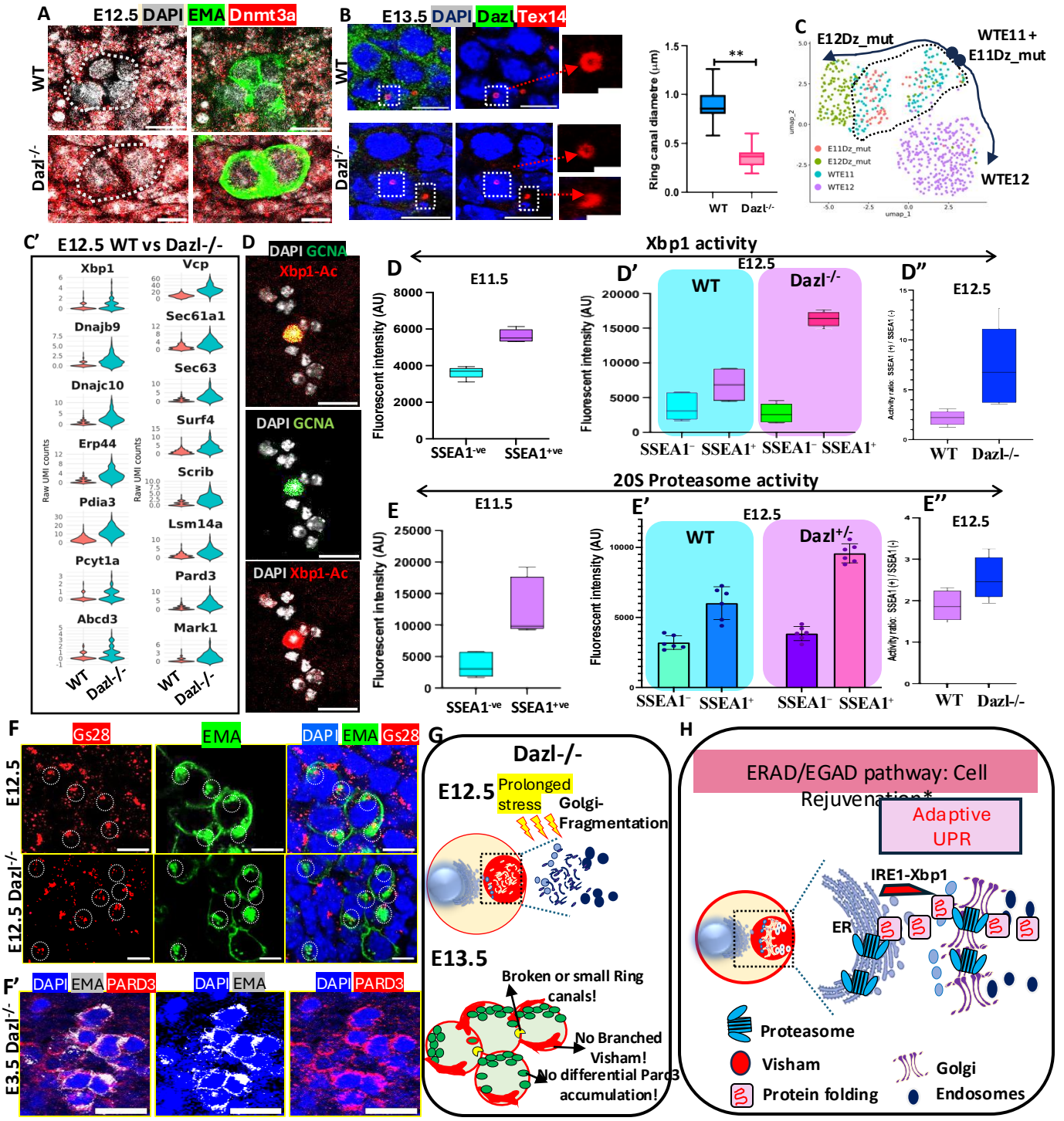
A
E12.5 DAPI EMA Dnmt3a
WT
Dazl-/-
B
E13.5 DAPI Dazl Tex14
WT
Dazl-/-
Ring canal diametre (µm)
**
WT
Dazl-/-
C
E12Dz_mut
WTE11 + E11Dz_mut
WTE12
E11Dz_mut
E12Dz_mut
WTE11
WTE12
umap_1
umap_2
C'
E12.5 WT vs Dazl-/-
Xbp1
Vcp
Dnajb9
Sec61a1
Sec63
Dnajc10
Surf4
Erp44
Scrib
Pdia3
Lsm14a
Pcyt1a
Pard3
Abcd3
Mark1
Raw UMI counts
WT
Dazl-/-
D
DAPI GCNA
Xbp1-Ac
DAPI GCNA
DAPI Xbp1-Ac
Xbp1 activity
D
E11.5
Fluorescent intensity (AU)
SSEA1-ve
SSEA1+ve
D'
E12.5
WT
Dazl-/-
SSEA1-
SSEA1+
D''
E12.5
Activity ratio: SSEA1 (+) / SSEA1 (-)
WT
Dazl-/-
20S Proteasome activity
E
E11.5
Fluorescent intensity (AU)
SSEA1-ve
SSEA1+ve
E'
E12.5
WT
Dazl+/-
SSEA1-
SSEA1+
E''
E12.5
Activity ratio: SSEA1 (+) / SSEA1 (-)
WT
Dazl-/-
F
Gs28
EMA
DAPI EMA Gs28
E12.5
E12.5 Dazl-/-
F'
DAPI EMA PARD3
DAPI EMA
DAPI PARD3
E3.5 Dazl-/-
G
Dazl-/-
E12.5
Prolonged stress
Golgi-Fragmentation
E13.5
Broken or small Ring canals!
No Branched Visham!
No differential Pard3 accumulation!
H
ERAD/EGAD pathway: Cell Rejuvenation*
Adaptive UPR
IRE1-Xbp1
ER
Proteasome
Visham
Protein folding
Golgi
Endosomes

Fig 5

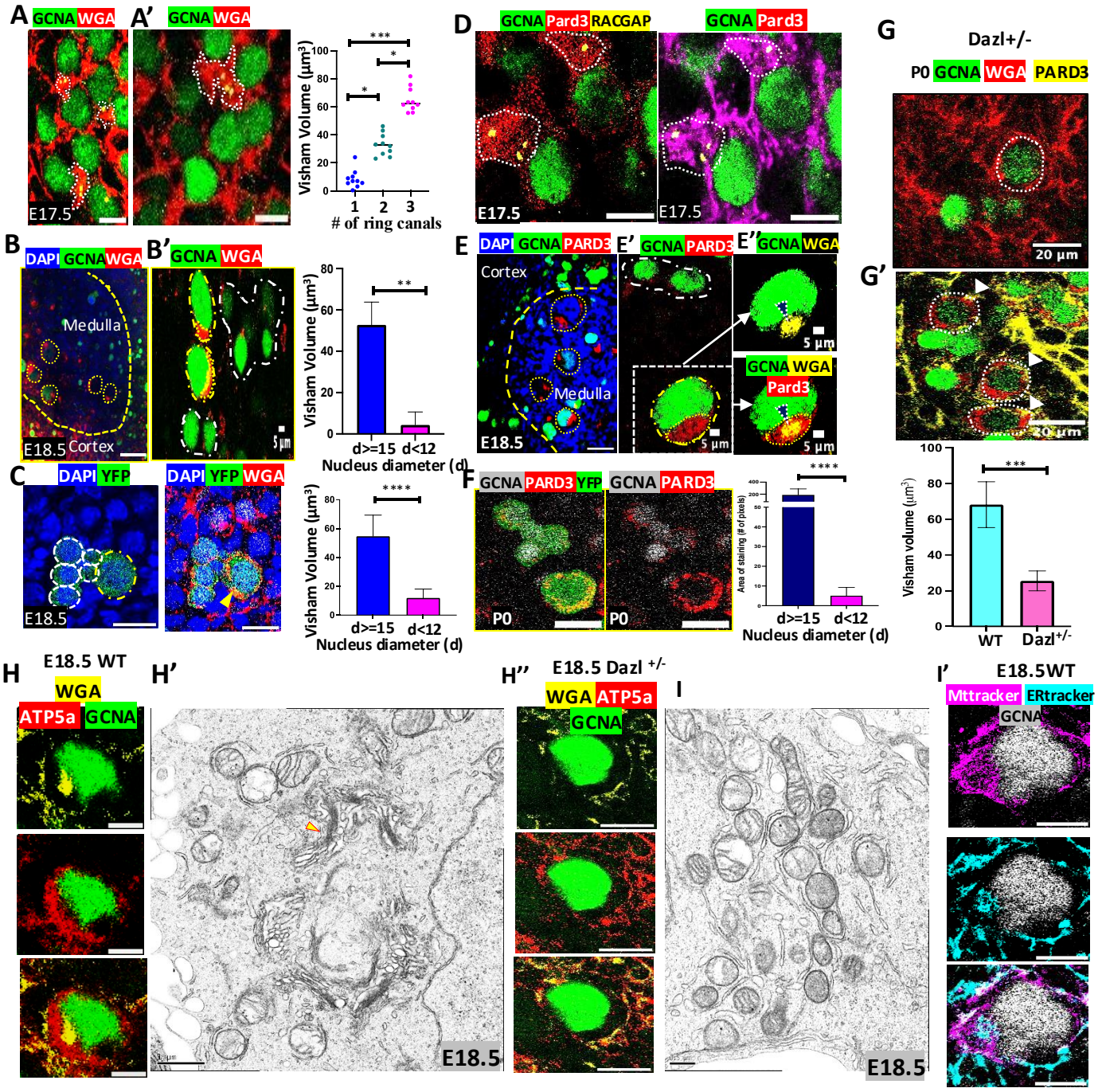
A
GCNA WGA
E17.5
A'
GCNA WGA
Visham Volume (µm³)
# of ring canals
B
DAPI GCNA WGA
Medulla
Cortex
E18.5
B'
GCNA WGA
5 µm
d>=15 d<12
Nucleus diameter (d)
C
DAPI YFP
DAPI YFP WGA
E18.5
D
GCNA Pard3 RACGAP
GCNA Pard3
E17.5
E
DAPI GCNA PARD3
Cortex
Medulla
E18.5
E'
GCNA PARD3
E''
GCNA WGA
GCNA WGA Pard3
5 µm
F
GCNA PARD3 YFP
GCNA PARD3
P0
Area of staining (# of pixels)
d>=15 d<12
Nucleus diameter (d)
G
Dazl+/-
P0 GCNA WGA PARD3
20 µm
G'
Visham volume (µm³)
WT
Dazl+/-
H
E18.5 WT
WGA
ATP5a GCNA
H'
E18.5
H''
E18.5 Dazl +/-
WGA ATP5a
GCNA
I
E18.5
I'
E18.5WT
Mttracker ERtracker
GCNA

Supplementary Videos and Figures

Fig. S1.

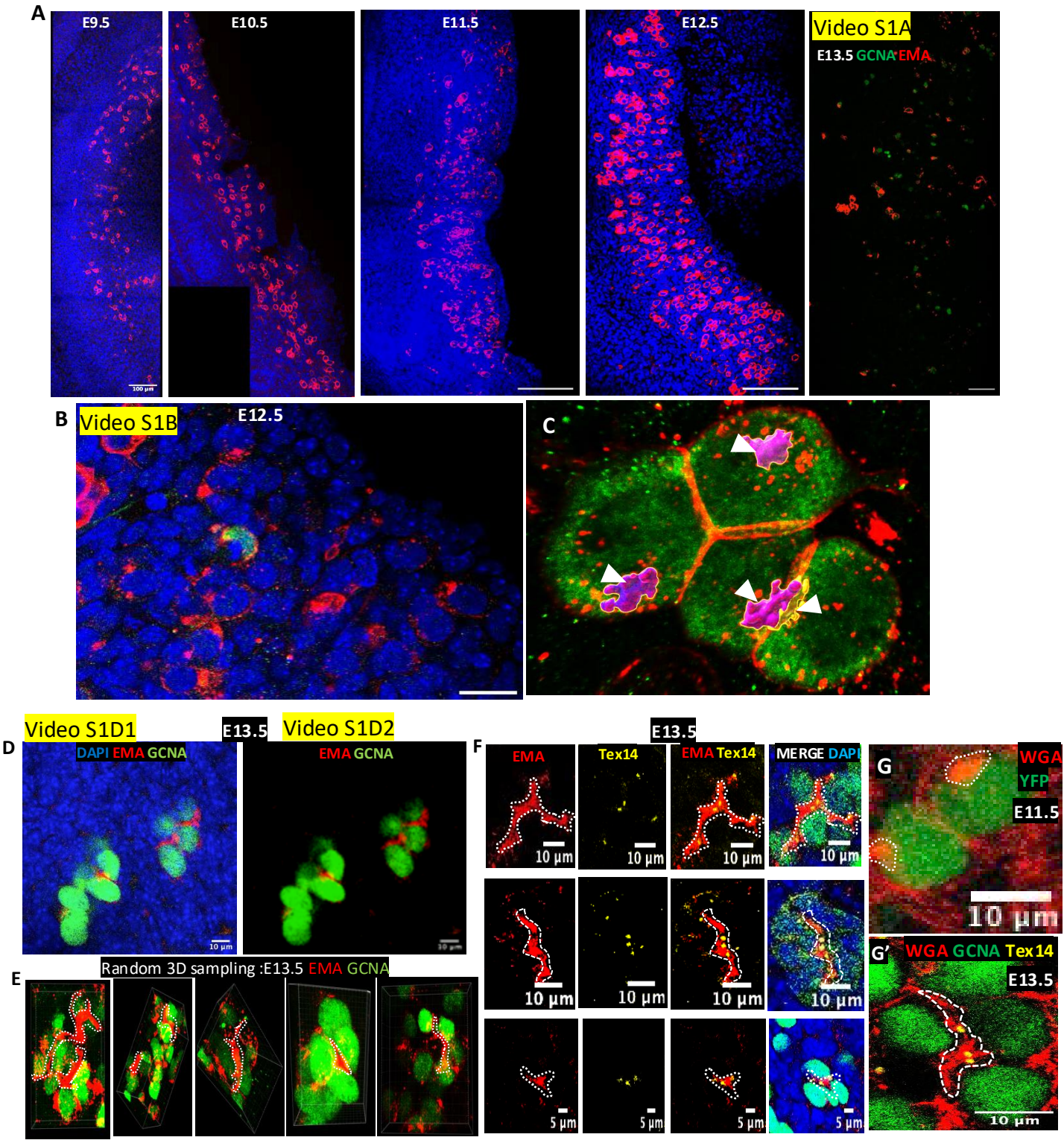
A
E9.5
E10.5
E11.5
E12.5
Video S1A
E13.5 GCNA EMA
B
Video S1B
E12.5
C
Video S1D1
E13.5
Video S1D2
D
DAPI EMA GCNA
EMA GCNA
E
Random 3D sampling :E13.5 EMA GCNA
F
E13.5
EMA
Tex14
EMA Tex14
MERGE DAPI
10 µm
5 µm
G
WGA
YFP
E11.5
G'
WGA GCNA Tex14
E13.5

Fig. S1 continued

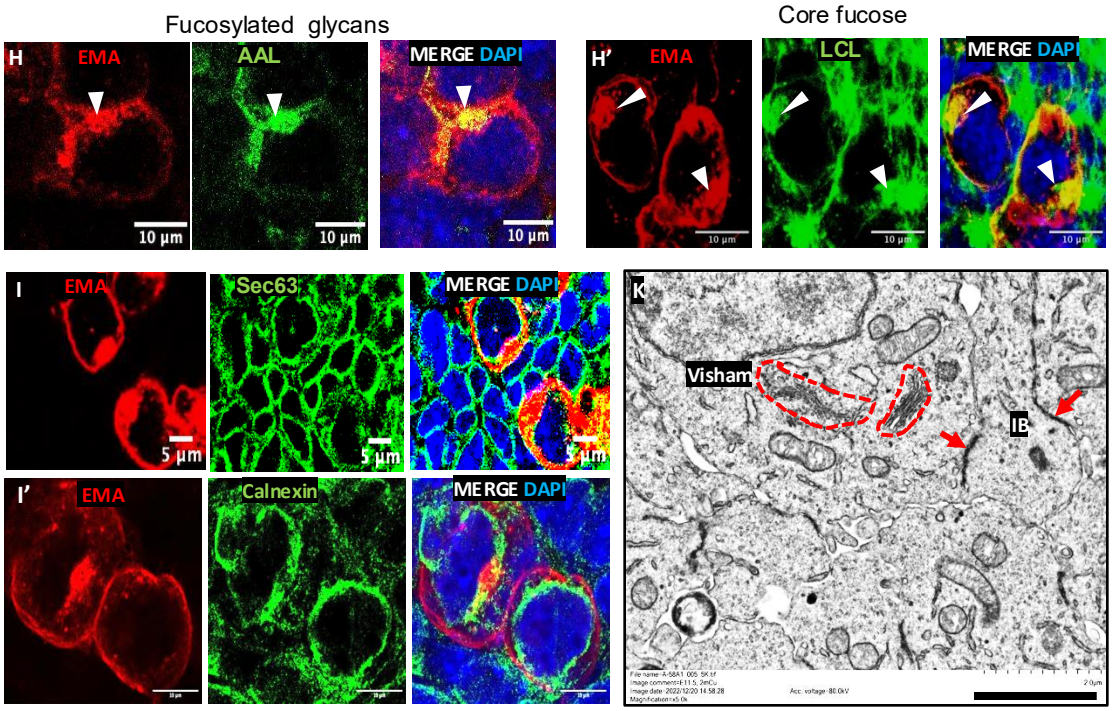

Fig. S2.

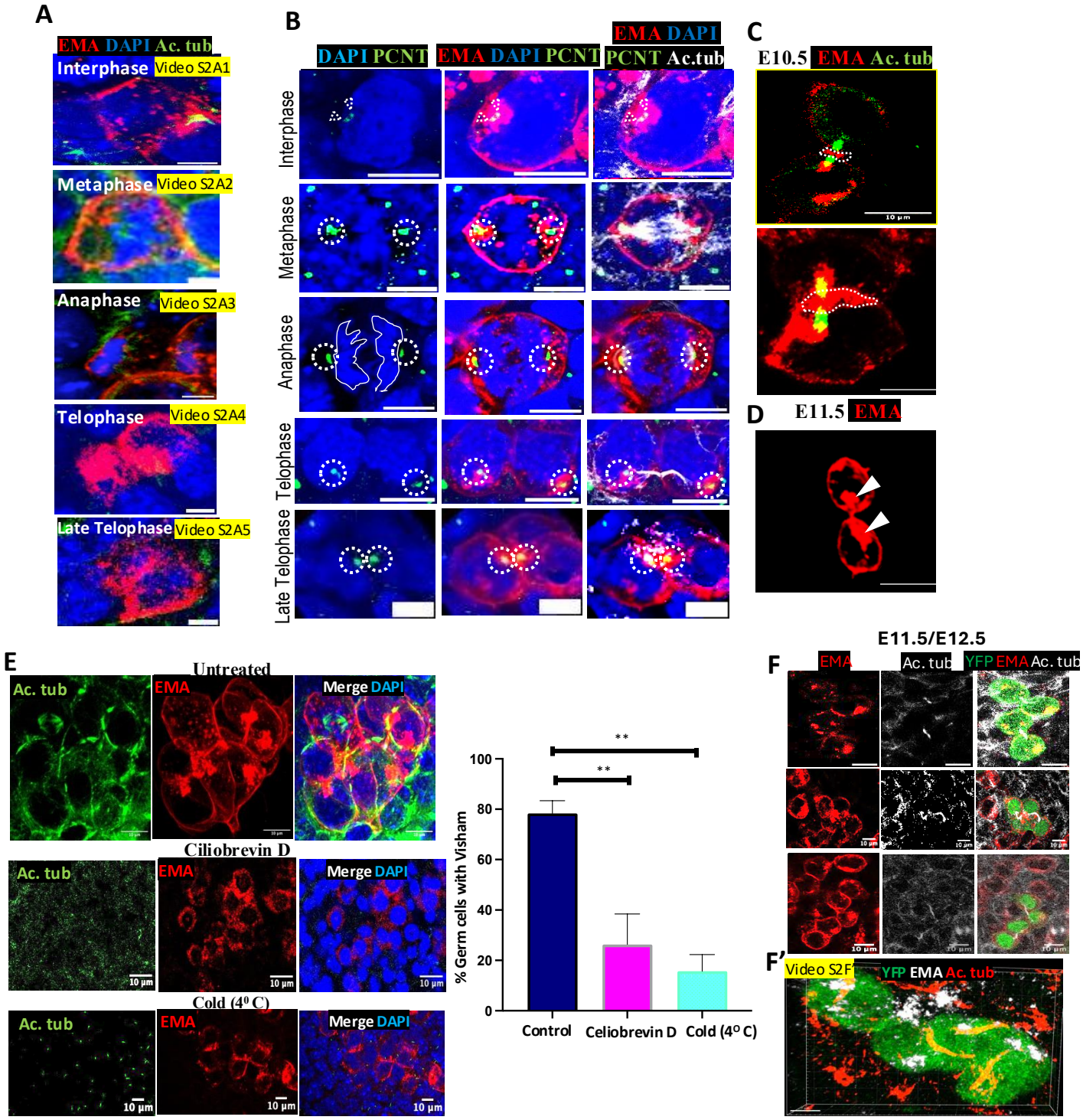
A
EMA DAPI Ac. tub
Interphase Video S2A1
Metaphase Video S2A2
Anaphase Video S2A3
Telophase Video S2A4
Late Telophase Video S2A5
B
DAPI PCNT
EMA DAPI PCNT
EMA DAPI
PCNT Ac.tub
Interphase
Metaphase
Anaphase
Telophase
Late Telophase
C
E10.5 EMA Ac. tub
10 µm
D
E11.5 EMA
E
Untreated
Ac. tub
EMA
Merge DAPI
Ciliobrevin D
Cold (4° C)
10 µm
% Germ cells with Visham
100
80
60
40
20
0
**
**
Control
Celiobrevin D
Cold (4° C)
E11.5/E12.5
F
EMA
Ac. tub
YFP EMA Ac. tub
F'
Video S2F'
YFP EMA Ac. tub

Fig. S3.

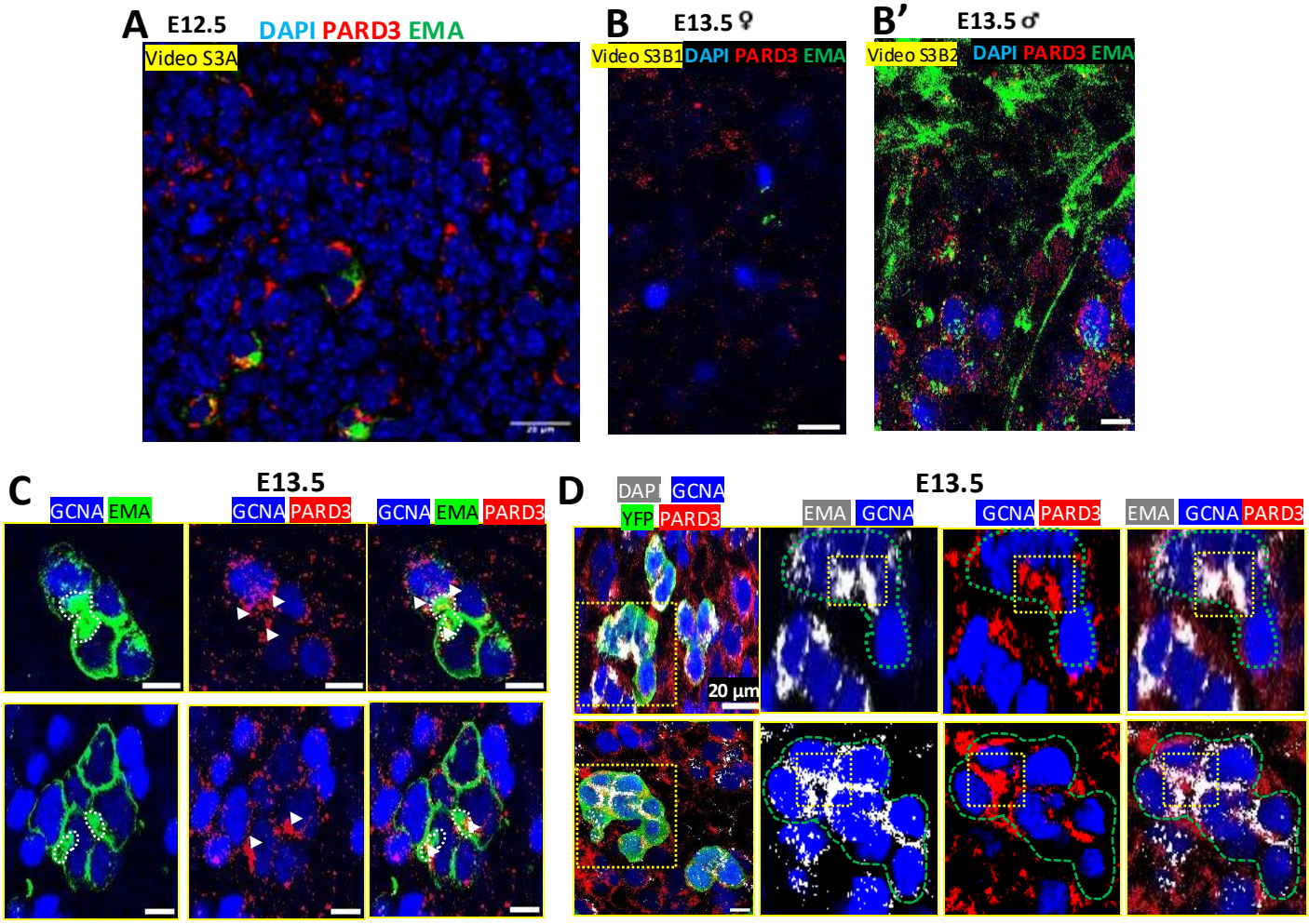
A
E12.5
DAPI PARD3 EMA
Video S3A
B
E13.5 ♀
Video S3B1
DAPI PARD3 EMA
B'
E13.5 ♂
Video S3B2
DAPI PARD3 EMA
C
E13.5
GCNA EMA
GCNA PARD3
GCNA EMA PARD3
D
E13.5
DAPI GCNA
YFP PARD3
20 µm
EMA GCNA
GCNA PARD3
EMA GCNA PARD3

Fig. S3 continued

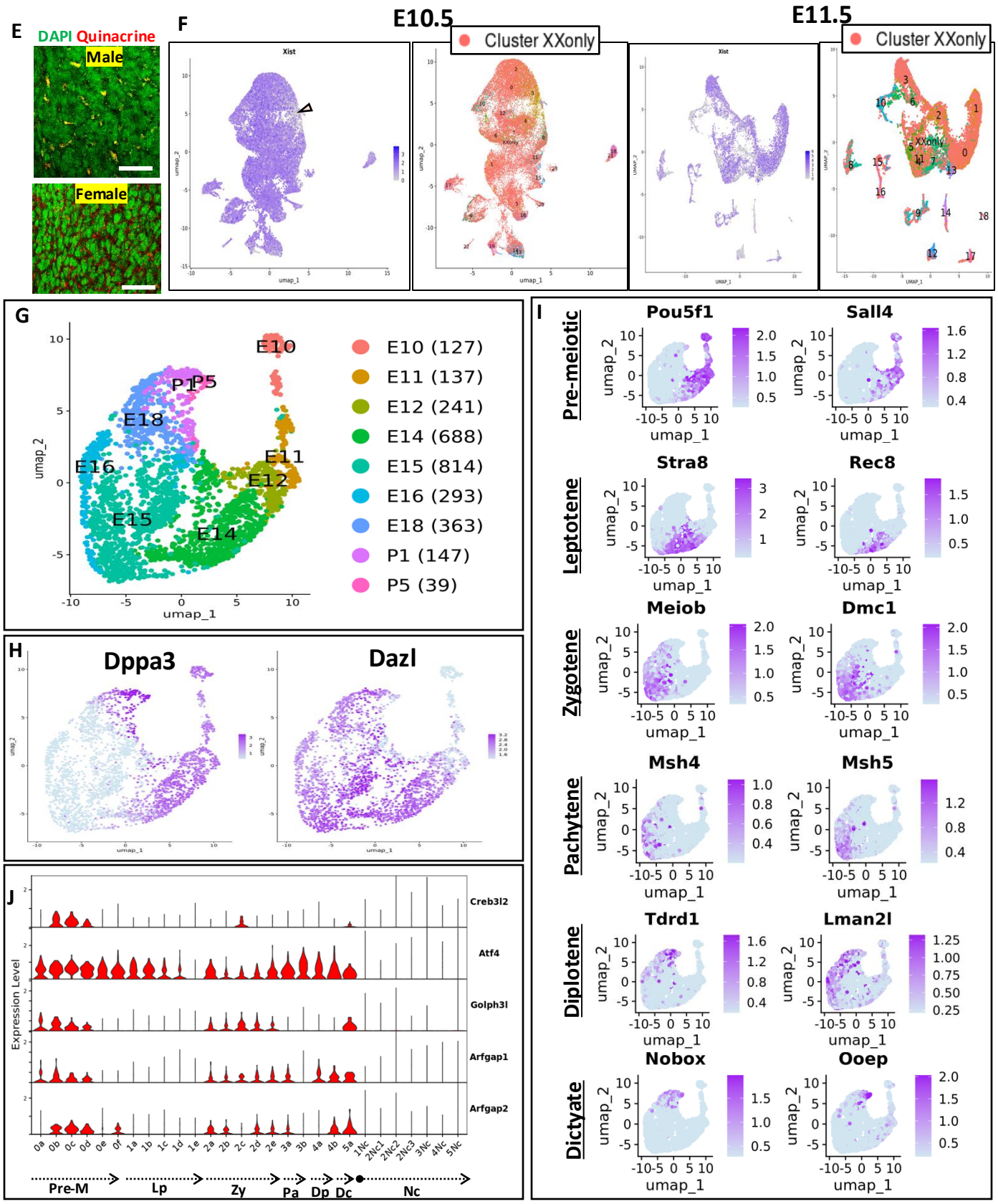

Fig S4.

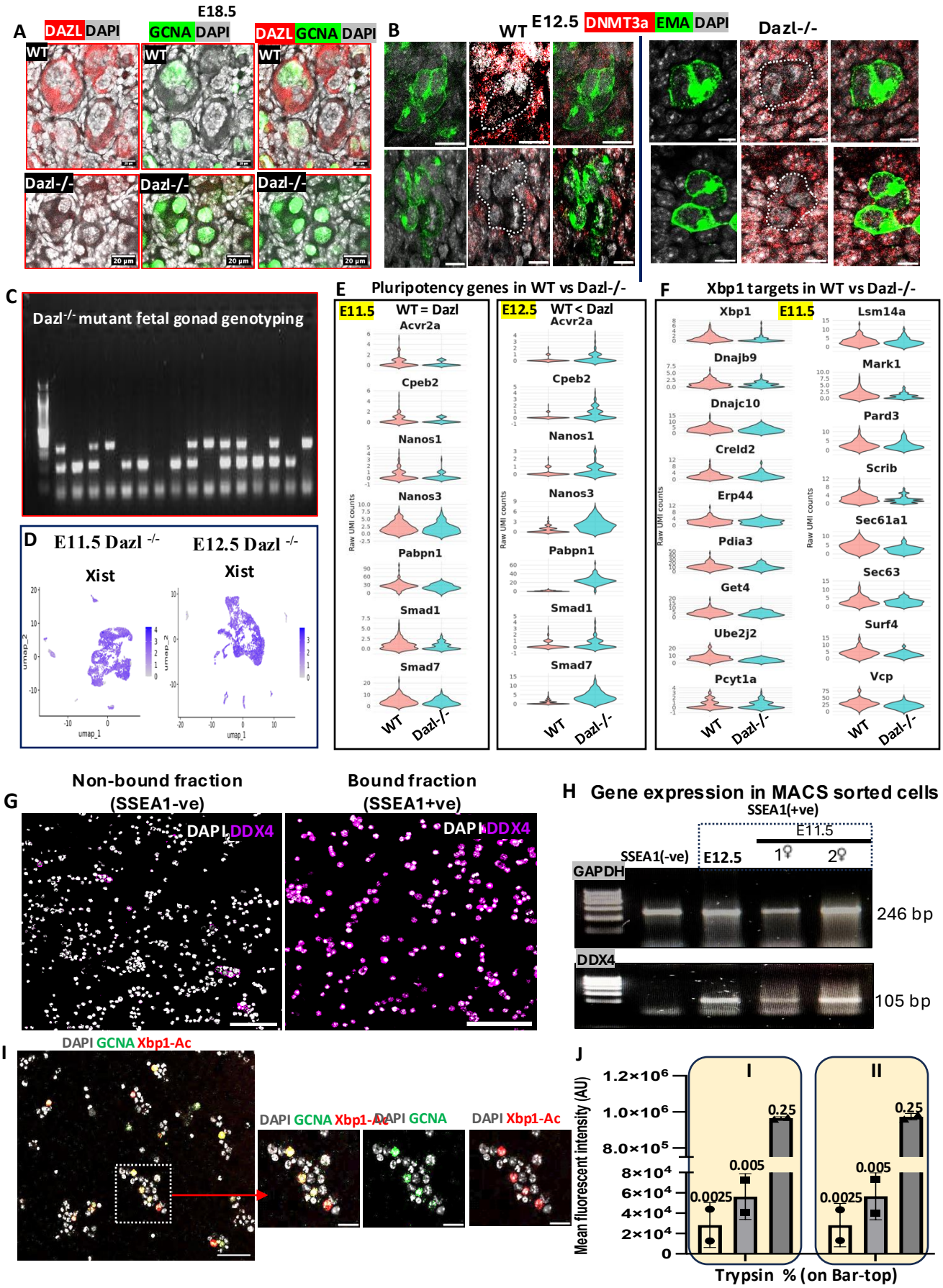
A
E18.5
DAZL DAPI
GCNA DAPI
DAZL GCNA DAPI
WT
Dazl-/-
20 µm
B
WT
E12.5
DNMT3a EMA DAPI
Dazl-/-
C
Dazl-/- mutant fetal gonad genotyping
D
E11.5 Dazl -/-
E12.5 Dazl -/-
Xist
umap_1
umap_2
E
Pluripotency genes in WT vs Dazl-/-
E11.5
WT = Dazl
E12.5
WT < Dazl
Acvr2a
Cpeb2
Nanos1
Nanos3
Pabpn1
Smad1
Smad7
Raw UMI counts
WT
Dazl-/-
F
Xbp1 targets in WT vs Dazl-/-
E11.5
Xbp1
Dnajb9
Dnajc10
Creld2
Erp44
Pdia3
Get4
Ube2j2
Pcyt1a
Lsm14a
Mark1
Pard3
Scrib
Sec61a1
Sec63
Surf4
Vcp
G
Non-bound fraction (SSEA1-ve)
Bound fraction (SSEA1+ve)
DAPI DDX4
H
Gene expression in MACS sorted cells
SSEA1(+ve)
E11.5
SSEA1(-ve)
E12.5
1♀
2♀
GAPDH
246 bp
DDX4
105 bp
I
DAPI GCNA Xbp1-Ac
DAPI GCNA
DAPI Xbp1-Ac
J
Mean fluorescent intensity (AU)
1.2×10⁶
1.0×10⁶
8.0×10⁵
8×10⁴
6×10⁴
4×10⁴
2×10⁴
0
I
II
0.25
0.005
0.0025
Trypsin % (on Bar-top)

Fig S5

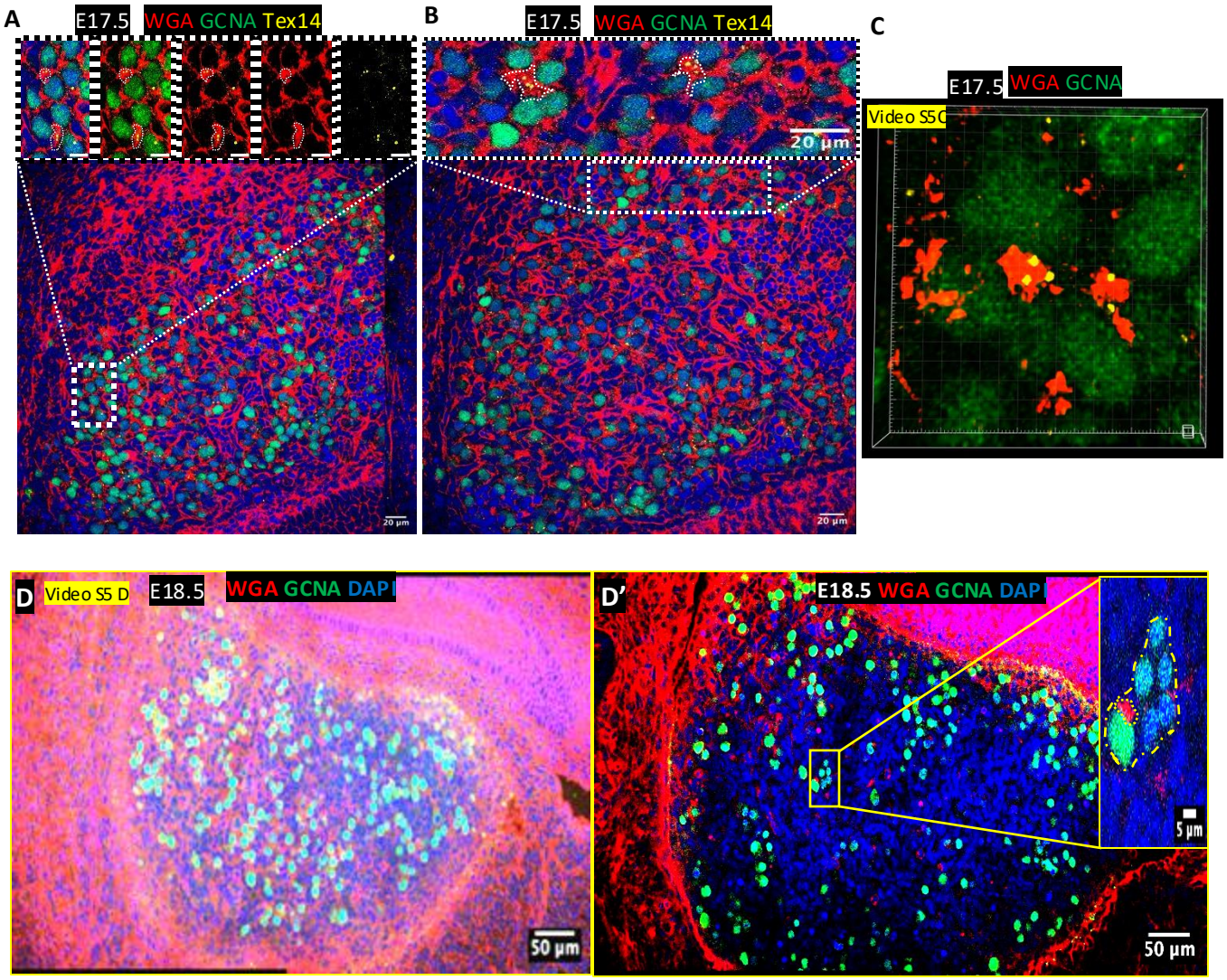
A
E17.5
WGA GCNA Tex14
20 µm
B
E17.5
WGA GCNA Tex14
20 µm
20 µm
C
E17.5
WGA GCNA
Video S5C
D
Video S5 D
E18.5
WGA GCNA DAPI
50 µm
D'
E18.5 WGA GCNA DAPI
5 µm
50 µm
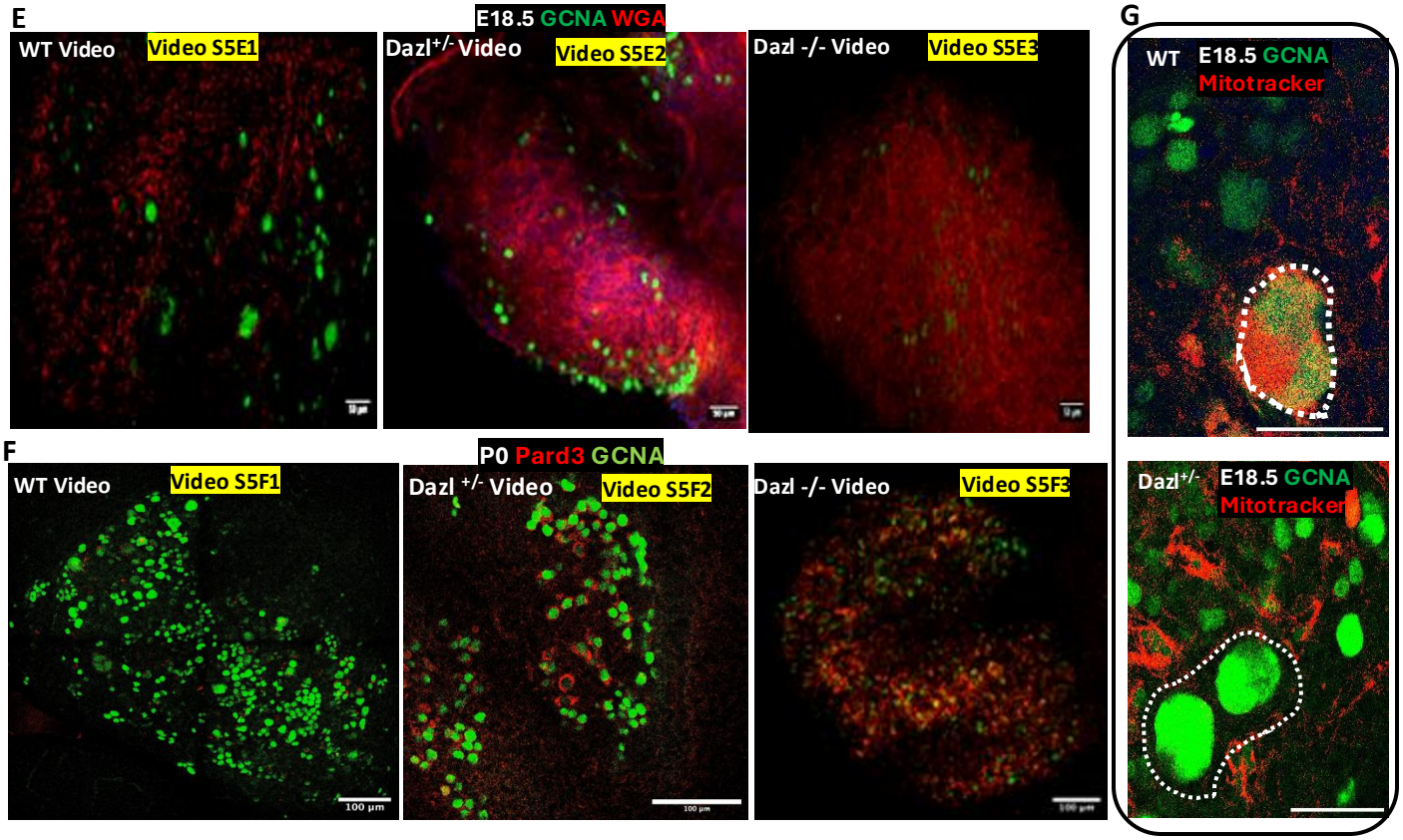
Fig S5 continued..